AGU PUBLICATIONS

Geochemistry, Geophysics, Geosystems

RESEARCH ARTICLE
10.1002/2015GC006240

New insights into lithology and hydrogeology of the northern Newark Rift Basin

N. V. Zakharova[1], D. S. Goldberg[1], P. E. Olsen[1], D. V. Kent[1,2], S. Morgan[1,3], Q. Yang[1], M. Stute[1], and J. M. Matter[1,4]

[1]Lamont-Doherty Earth Observatory, Columbia University, Palisades, New York, USA, [2]Earth and Planetary Sciences, Rutgers University, Piscataway, New Jersey, USA, [3]Department of Geology, University of Leicester, Leicester, UK, [4]Ocean and Earth Science, National Oceanography Centre, Southampton University, Southampton, UK

Key Points:
- Marginal facies of the Stockton Formation show no continuity over 200 m lateral distance
- Despite a predominance of coarse sandstones, hydraulically conductive zones are sparse
- Coring of crystalline basement below the Newark basin showed it to be the Fordham gneiss

Correspondence to:
N. V. Zakharova,
nzakh@ldeo.columbia.edu

Citation:
Zakharova, N. V., D. S. Goldberg, P. E. Olsen, D. V. Kent, S. Morgan, Q. Yang, M. Stute, and J. M. Matter (2016), New insights into lithology and hydrogeology of the northern Newark Rift Basin, *Geochem. Geophys. Geosyst.*, *17*, doi:10.1002/2015GC006240.

Received 24 DEC 2015
Accepted 1 MAY 2016
Accepted article online 9 MAY 2016

Abstract The marginal facies of the Triassic rift basins in the eastern United States are poorly documented, particularly on the hinge or hanging wall margins. This study presents a lithological description and multiscale petrophysical analysis of basement rocks, overlying marginal facies of the early synrift strata, and the basal contact of the Palisade Sill that were drilled and cored in the northeastern part of the Newark Basin, near its terminus. The expression of the Stockton Formation differs from that in the central basin in having thinner layers, with uncertain temporal relationship to the type area. The bottom 50 m is lithologically distinct with brick-red to dark-purple mudstones and sandstones, abundant gypsum-filled fractures, and a thin zone with anomalously high uranium concentration, not associated with organic-rich mudstones as other occurrences in the basin. The crystalline basement is apparently Fordham gneiss, overlain by a thin sandstone layer and a dark-purple hydrophilic mudstone. Despite the abundance of coarse-grained strata and multiple sets of tectonic fractures, hydraulically transmissive zones are sparse, and do not uniquely correlate to fracture and/or matrix characteristics. Enhanced transmissivity may exist along intrusion boundaries due to enhanced thermal fracturing, but more hydraulic data are needed to verify it. Comparison of petrophysical data in two boreholes ~210 m apart shows no direct correlation of individual lithological units and their hydraulic properties, although the overall formation characteristics are similar. The results highlight challenges for outcrop correlation at the marginal edges of the rift basins and estimating reservoir properties of these heterogeneous formations.

1. Introduction

The Newark Rift Basin, formed during the breakup of Pangaea in the early Mesozoic, is one of the largest of exposed rift basins in eastern North America [*Withjack et al*., 2013; *Olsen et al*., 1989]. It has a classic half-graben structure bounded by northeast-trending normal faults along the northwestern boundary (Figure 1a). Despite significant postdeposition erosion, the preserved basin is filled with over 7 km-thick section of Late Triassic to Early Jurassic continental sedimentary rocks and mafic igneous rocks [*Olsen et al*., 1996; *Schlische*, 1992]. The igneous rocks belong to the Central Atlantic Magmatic Province (CAMP) and are represented by both extrusive flows and intrusive bodies, most notably, the Palisade diabase Sill [*Marzoli et al*., 1999; *Puffer et al*., 2009]. Extensive studies of the Newark basin's structure and lithology have significantly contributed to the understanding of development and evolution of the Mesozoic rift system and concurrent environmental conditions in eastern North America [e.g., *Withjack et al*., 2013; *Blackburn et al*., 2013; *Olsen and Kent*, 1996; *Schlische*, 1992; *Smoot*, 1991]. Located in the densely populated and industrialized area of southeastern New York, New Jersey and Pennsylvania (Figure 1a), the Newark Basin was also a focus of numerous studies on groundwater resources and pollution remediation in fractured aquifers [*Heisig*, 2011; *Lacombe and Burton*, 2010; *Morin et al*., 2000; *Morin et al*., 1997; *Houghton*, 1990]. In recent years, it has been considered as a potential CO_2 storage site in the framework of Carbon Capture and Storage (CCS), one of the solutions for reducing anthropogenic CO_2 emissions into the atmosphere [e.g., *Intergovernmental Panel on Climate Change (IPCC)*, 2005; *Lackner*, 2003; ; *Matter et al*., 2007]. As a part of concentrated effort by the U.S. Department of Energy (DOE) in partnerships with major private and state organizations, multiple sedimentary basins throughout the country are being assessed for CO_2 storage potential [e.g., *Rodosta et al*., 2011; *Litynski et al*., 2009]. On the eastern North American margin they include the onshore Mesozoic

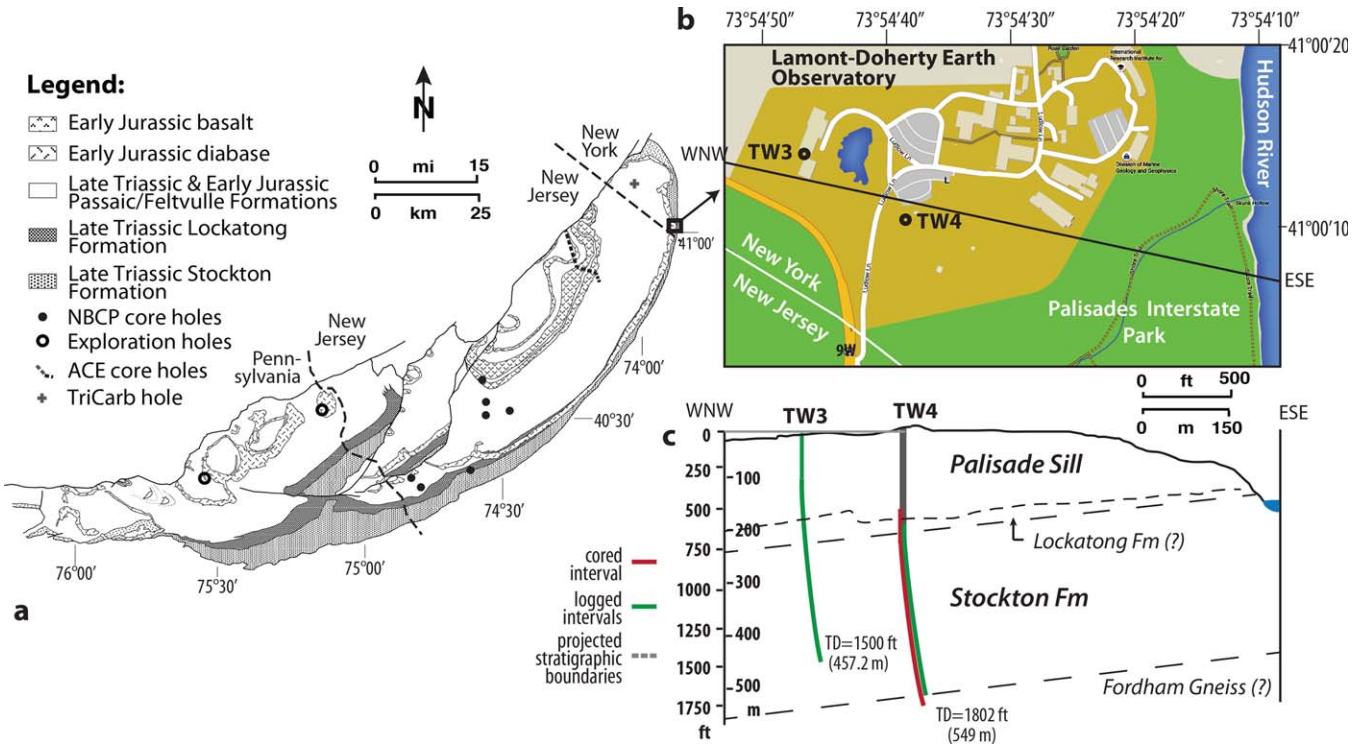

Figure 1. The study site location in the northeastern Newark Basin: (a) Geologic map of the Newark Basin showing the location of previous coring sites (the Newark Basin Coring Project (NBCP), the U.S. Army Corps of Engineers (ACE), the TriCarb Consortium for Caron Sequestration drill hole, and industry exploration holes). The square box at the top right indicates the location of this study. (b) A map of the study site on the campus of Lamont-Doherty Earth Observatory showing the position of two test wells described in this study: the Test Well-3 (TW3) and Test Well-4 (TW4). (c) Schematic cross-section through the study site along the WNW-ESE line. Depth is reported in driller's units (ft) below the ground level at the well heads, here plotted along the metric scale. The ground level at TW4 wellhead is 10 ft (~3 m) higher than TW3 wellhead. The test wells are located roughly 210 m (~700 ft) apart along the sedimentary strata's dip direction (~10 degrees to NW). Both wells deviate 0–5° from vertical in the updip direction. The exact geometry of the stratigraphic boundaries between the wells and at the Hudson River is not known, but a projection based on observed boundaries and their dips in the wells is shown by the dashed lines.

Newark Rift Basin and offshore South Georgia Rift Basin, thought to be the largest on this margin but buried below the Cretaceous-Cenozoic Coastal Plain sediments of South Caroline, Georgia, Alabama and Florida [*Akintunde et al*., 2014, 2013]. The advantages of Newark basin include its proximity to many CO_2 emitters [e.g., *Goldberg et al*., 2010; *Tymchak et al*., 2011], easy accessibility, and significant amount of information about the basin accumulated in prior studies, which included studies of field outcrops [e.g., *Olsen*, 1980; *Cornet and Olsen*, 1985], core holes [e.g., *Kent et al*., 1995; *Olsen et al*., 1996; *Reynolds*, 1994], and seismic-reflection surveys [*Costain and Coruh*, 1989; *Reynolds*, 1994; *Withjack et al*., 2013]. Most of those projects, however, focused on the central part of the basin, characterized by the thickest and most complete sedimentary record. The record there is dominated by fine-grained strata of the Lockatong and Passaic Formations that have long been recognized as largely lacustrine in origin [*Van Houten*, 1969; *Olsen et al*., 1996; *Smoot*, 1991, 2010], which are expected to have poor reservoir properties. Basin edges, on the contrary, received much less attention, but are projected to host coarse-grained deposits of the predominantly fluvial Stockton Formation, the most hydraulically conductive among Newark basin formations [*Herman*, 2010], and potentially, permeable basal conglomerates at the basement contact [e.g., *Smoot*, 1991, 2010].

Very little is known about the Newark Basin edges, especially about subsurface geology and petrophyscial formation properties at the northern onlap tip of the basin. Outcrops occurring here, e.g., along the Hudson River under the Palisade Sill and along the New York State Thruway, have very limited spatial extent. They do not provide a clear picture of mutual relationship of different sedimentary units, which appear to be very diverse in this area. Using basin-wide projections and seismic survey data from the central basin, equivalents of the Lockatong and upper Stockton Formations are inferred to rest unconformably on Paleozoic and/or Proterozoic basement rocks in the northern basin edge [*Schlische*, 1992]. The basement was inferred to extend from the Manhattan prong across the Hudson valley, but its depth is poorly constrained. The groundwater wells, though abundant in the region, are shallow (total depth less than 150 m [*Heisig*, 2011]),

and important reservoir properties such as porosity and permeability in deeper formations (below shallow groundwater) are not known. Therefore, our knowledge about the geology of the northern basin edge, our understanding of key parameters needed for evaluating the basin's CO_2 storage potential, and our insight into the lithology and hydrogeology of the basin edge have previously been limited. This study starts filling this gap by providing core and borehole data to address the structure, lithology, and fracture hydrology at the northeastern basin edge, and the lateral extent of lithological and hydraulic features at depths below potable groundwater resources. To the best of our knowledge, no such information has been published for this part of the basin to date.

This paper presents the first description of intact basement rocks and early synrift strata below the Palisade Sill at the northeastern basin edge based on >350 m of continuous core description, analysis of core and downhole physical properties, and correlation of physical and hydraulic properties in two wells located ~210 m apart. These data were accumulated through multiple projects conducted over the years on the campus of Lamont-Doherty Earth Observatory (LDEO), Columbia University in Palisades, NY (Figure 1). They include an early study of the Palisade Sill and contact zone support by LDEO and the Earth Institute of Columbia university [*Matter et al*., 2006; *Goldberg and Burgdorff*, 2005], an EPA-supported study of the biochemical effects of a simulated CO_2 leak into shallow aquifers [*O'Mullan et al*., 2015; *Yang et al*., 2014], and most recent drilling by the TriCarb Consortium for Carbon Sequestration aiming at characterization of the Newark Basin for CO_2 geologic storage [*Slater et al*., 2012; *Tymchak et al*., 2011; *Olsen et al*., 2011]. The goal of this work is to integrate these multidisciplinary (geology, geophysics and hydrogeology) and multiscale (core to cross-borehole) data sets, and to provide a unified picture of basin geology at this location, leading to new insights into the geologic setting of the northeastern Newark Basin.

2. Study Site and Methods

2.1. Brief Description of the Newark Basin and the Study Site Location

The major lithostratigraphic units of the Newark basin are sedimentary Stockton, Lockatong and Passaic Formations of Late Triassic age, followed by a series of basalt flows interbedded with sedimentary formations of latest Triassic-Early Jurassic age (the Orange Mountain Basalt, the Feltville Formation, the Preakness Mountain Basalt, the Towaco Formation, the Hook Mountain Basalt, and the Boonton formation). Aside from the predominantly fluvial Stockton Formation (composed of conglomerates, arkose, and sandstone, and mudstone units), and marginal coarse clastics near the border faults, most of the basin sedimentary strata are lacustrine, and exhibit systematic cyclicity in sediment fabric, color and total organic content that reflects fluctuations in lake levels driven by Milankovitch cycles [*Olsen*, 1986*; Olsen and Kent*, 1996]. The Lockatong Formation is distinguished by a predominance of fine-grained gray to black mudstones, while the Passaic Formation is characterized by mostly red mudstone and sandstone units with subordinate gray and black units [*Olsen et al*., 1996]. The younger three sedimentary sequences consist predominantly of fluvio-lacustrine, red clastic rocks interbedded with gray and black deeper-water lacustrine rocks.

The Newark basin underwent significant postdeposition erosion that exposed its major units and internal structures [*Withjack et al*., 2013; *Malinconico*, 2009; *Schlische*, 1992]. Basin strata generally dip 5–15° WNW toward the basin-bounding fault system that consists of a series of northeast-striking, southeast-dipping right-stepping normal fault zones. The majority of large-scale structures, such as intrabasinal faults and dykes, strike in the northeastern direction, subparallel to the border fault and perpendicular to the regional direction of extension during the basin formation [*Schlische*, 1992]. The principal strike direction for fractures and joints is also to the northeast, but fracture distribution and orientation vary throughout the basin [*Herman*, 2009; *Morin et al*., 1997]. Fractured-rock aquifers define the principal groundwater system in the basin [*Lacombe and Burton*, 2010; *Houghton*, 1990].

The study site is located in the northern part of the Newark basin on the campus of Lamont-Doherty Earth Observatory (LDEO), Columbia University in Palisades, NY (Figure 1b). The campus is situated on the western side of the Hudson River immediately north of the New York-New Jersey border, on the outcropping Palisade Sill. The data presented here were collected in two boreholes: Test Well-3 (TW3: 41.00398°N, 73.91268°W) and Test Well-4 (TW4: 41.00292°N, 73.91061°W), located roughly 700 ft (~210 m) updip from TW3 (Figure 1c). Both wells intersected the outcropping Palisade Sill and underlying sedimentary strata of the Newark basin, and TW4 also penetrated the crystalline basement below the basin. The depth of core

and borehole data was measured from the ground level (GL); GL elevation is 380 ft (116 m) at TW3 wellhead and 389 ft (118.5 m) at the TW4 wellhead.

2.2. Drilling and Coring

TW3 was initially drilled to a depth of 1000 ft (305 m), intersecting the Palisade Sill and contact-metamorphosed sedimentary strata below it, described by *Goldberg and Burgdorff* [2005] and *Matter et al*. [2006]. For this study, TW3 was deepened to the total depth (TD) of 1500 ft (457 m) to allow for characterization of unaltered sedimentary rocks of the Stockton Formation. Both drilling phases were performed without coring but with drill cutting collection roughly every 5 ft (1.5 m) of bit advance to inform lithological identification of the penetrated formations [*Shao*, 2011; *Goldberg and Burgdorff*, 2005]. The nominal (bit size) diameter of TW3 is 6.25 in (∼15.6 cm). The hole slightly deviates from vertical toward a perpendicular to the bedding, gradually increasing the deviation angle with depth from 0 to the maximum deviation of 5 degrees at TD in the east-southeast direction. Twenty feet (6 m) of casing is installed at top and capped, but the majority of the hole remains open.

The drilling of TW4 was conducted in 3 phases. First, the upper 646 ft (∼197 m), all within the Palisade Sill, were drilled without coring but with drill cuttings collection every 10 ft (∼3 m) of bit advance. Then, from 646 ft to 750 ft (196.8–228.6 m) drilling continued with coring using a 4.88 in wide (∼12.2 cm) PQ diamond bit. The first sedimentary rocks below the sill were encountered at a depth of 691 ft (210.6 m). At 750 ft (228.6 m) drilling stopped, and the hole was cased, and the casing cemented in order to protect shallow aquifers. Below 750 ft, drilling and coring continued with a 3.84 in wide (9.6 cm) HQ bit. The crystalline basement was penetrated at a depth of 1711 ft (521.5 m), marking the first drilling into the basement in the northern Newark basin. TW4 remains open from below the casing to approximately this depth. TW4 was drilled to a total depth of 1802 ft (∼550 m) and then capped. Core recovery was close to 100% (1156 ft, or 352 m of core collected), with only a few thin zones of rubble. The hole deviates slightly ($\leq$3 degrees) to the east-southeast, toward a perpendicular to the bedding.

2.3. Core Description and Analysis

The TW4 core lithology was described by a detailed visual analysis. Each distinct unit was assigned a numerical index for color and grain size. The scale for color is: −1—white, 0—red, 1—purple, 2—gray, 3—black, with intermediate shades described by fractions of these numbers. The grain size scale varies from 0 (claystone) to 8 (medium conglomerate), with intermediate values as annotated in figures. Throughout the paper we plot a composite lithological log for TW4 core that combines color and grain size in a single column, with its width corresponding to the core grain size and the color converted to RGB scale quantitatively scaling core color index to RGB expression of white, red, purple, gray, and black. In addition, notable features observed in the core are provided as annotation on the litho-column. Visual core description was complemented by laboratory measurements on select core plugs conducted at Weatherford Laboratories as part of the TriCarb project. Those included basic XRD mineralogy and routine core analysis of porosity, air permeability and grain density [e.g., *Slater et al*., 2012].

In order to directly correlate core lithology to formation physical properties, core physical properties were measured continuously with Multi-Sensor Core Logger (MSCL) at Lamont-Doherty Earth Observatory, allowing for nondestructive, noninvasive high-resolution measurements of gamma density, approximating the bulk density, and magnetic susceptibility (MS) on the whole rock cores. The measurements were made at room temperature (∼20°C) with a sampling interval of 0.8 in (2 cm), and were corrected for core diameter and temperature variations. The gamma density was measured using ^{137}Cs source, calibrated daily using a stepped aluminum density standard. The whole-core magnetic susceptibility was measured with a Bartington MS2 system using different loop sizes for the wide PQ cores (top 100 ft of TW4 core) and the HQ core (the majority of TW4 core). The MS sensor has two fixed sensitivity levels, 0.1 kHz and 1.0 kHz, which correspond to count times of 10 s and 1 s respectively. The higher sensitivity level of 0.1 kHz/10 s was used for the majority of the cores, notably the Newark Basin sedimentary rocks, due to the low- to moderate-levels of magnetic susceptibility of those cores. The quicker, lower sensitivity setting (1 kHz/1 s) was used for the Palisade Sill transition and the metamorphic basement cores. The system was calibrated daily with loop-specific calibration check pieces provided by manufacturer. The sensor automatically zeroes itself and takes a free air reading at the start and end of each run in order to account for instrument drift by subtraction of a linear interpolation between readings. MS data were recorded as corrected volume specific units (10^{-5} SI)

and therefore did not account of the density of the sample being measured. Variations in the core's density as a result may be reflected in the magnetic susceptibility data.

In addition, high-resolution spectral gamma ray (SGR) measurements were acquired for a core interval with anomalously high total gamma ray counts at ~1594 ft/485.9 m. The core SGR acquisition system (Canberra model 802) at Rutgers University consisted of a gamma ray detector (2x2 in/5x5 cm cylindrical NaI(Ti) crystal) and photomultiplier tube housed in a lead shield. Gamma rays were registered in 2048 spectral channels corresponding to the energy range from a few keV to ~3200 keV. Spectral calibration was performed using a mixed nuclide standard source with known emission lines for ^{109}Cd, ^{137}Cs, and ^{60}Co [*Lanci et al*., 2002]. Background SGR level produced by cosmic rays and potential impurities and contamination in the acquisition system was measured and subtracted from the results. The natural gamma ray spectrum of rock and soils is composed of one emission peak of potassium (^{40}K) at 1460 keV, and more than a dozen emission peaks of uranium (^{238}U) and thorium (^{232}Th) series. Uranium and thorium emission peaks correspond to its daughter products, rather that the elements themselves. By comparing core SGR spectra to independently measured elemental abundances of K, U, and Th, *Blum et al*. [1997] showed that within the measured SGR range, uranium is best identified by its daughter product ^{214}Bi with emission peaks at 610, 1120 and 1764 keV, and thorium by it daughters ^{228}Ac and ^{208}Tl at 912–966 keV and 2615 keV, respectively. These characteristic peaks were used to interpret high total gamma ray activity detected in TW4 core.

All core labels, core logs, and borehole logs were recorded and archived in decimal feet, an engineering variant of the English system units used in drilling industry. Thus, all further depth references in this paper are provided in decimal feet to facilitate the retrieval and usage of these data in further research.

2.4. Wireline Logging and Hydraulic Testing

Conventional petrophysical and flowmeter measurements were collected in the open-hole sections of both boreholes. In TW3, the logging data were recorded from the surface to TD, and span the Palisade Sill and basin sedimentary strata (Figure 1c). In TW4, a bridge formed soon after drilling through the incompetent layers (dark purple strata) above basement and the logging tools were unable to pass; therefore, petrophysical and hydraulic data in TW4 are limited to the open-hole sedimentary section from 750 ft to 1690 ft (228.6–515.1 m) (Figure 1c). The measurements include a three-arm caliper (borehole diameter), natural gamma ray, short-normal (16 in, or 40 cm) and long-normal (64 in, or 160 cm) resistivity, magnetic susceptibility, optical and acoustic televiewers, and borehole fluid resistance and temperature logs. Electromagnetic (EM) vertical flowmeter (0.05–40 L/min sensitivity range) was run under ambient conditions, and during water injection at the rate of 11.4 L/min. In TW3, a heat-pulse (HP) vertical flowmeter was employed in addition to an EM flowmeter to achieve better accuracy over the low-transmissivity range (0.113–3.785 L/min). Water levels were continuously monitored using a pressure transducer. Trasmissivity of fractured zones was evaluated from the water-level and flowmeter logs assuming steady-state flow conditions [*Day-Lewis et al*., 2011]. In TW4, however, true steady state flow was not achieved (the borehole water level rose from 389 ft to 243 ft (118.5 to 74 m) over 4 h of injection), and the computed transmissivity values are likely overestimated.

Interactive analysis of bedding and fractures was conducted using optical (OTV) and acoustic (ATV) borehole televiewers that both provide azimuthally oriented 360°-view of the borehole walls. The optical televiewer proved to be particularly effective in these small-diameter, water-filled boreholes, and allowed for the identification of many millimeter-to-centimeter-scale features not visible in acoustic images. A nearly true color depiction of sedimentary features in OTV images aided in identification of lithostratigraphic units in TW3 and refining their depths first determined from drill cutting analysis. OTV images in TW4 were in excellent agreement with core description, and were used for TW3–TW4 cross-hole lithological correlation. In fracture analysis, however, borehole images and core data produce a bias in sampling statistics toward low-angle fractures. This bias stems from the fact that the probability of intersecting near-horizontal fractures with a vertical borehole is higher than the probability of intersecting subvertical fractures. Therefore, the relative abundance of low-angle fractures is likely to be overestimated compared to their true relative frequency [*Terzaghi*, 1965]. To account for such sampling bias, a geometrical correction in the form of $1/\cos\theta$, where θ is a measured fracture dip angle, was applied to all fracture populations determined from borehole images [e.g., *Barton and Zoback*, 1992; *Morin et al*., 1997]. The corrected populations predict the

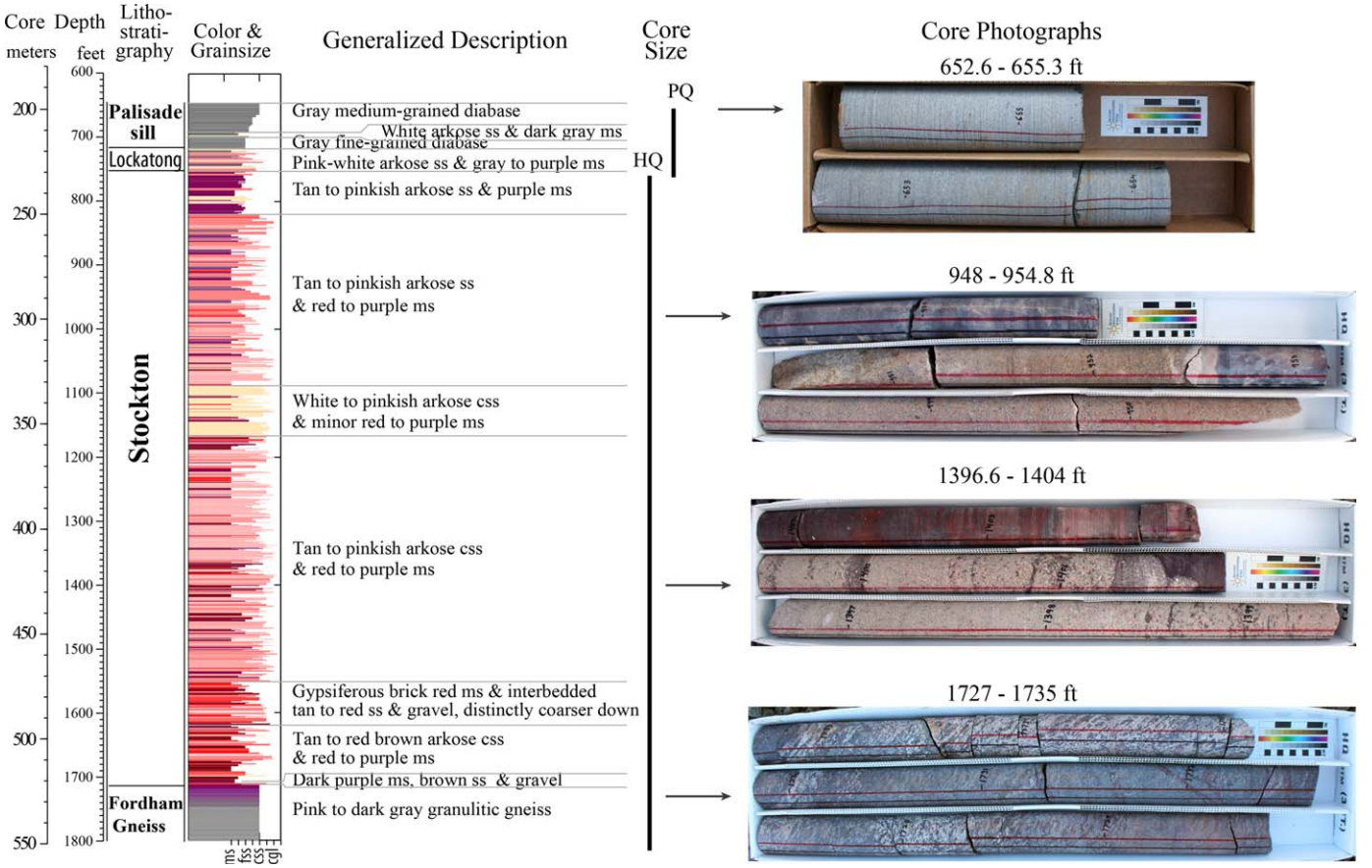

Figure 2. Lithological description of the TW4 core. From left to right: depth of the core, lithostratigraphic units, color and grain size of individual strata (ms—mudstone, fss—fine sandstone, css—coarse sandstone), core size, and photographic images of representative core intervals.

frequency of fractures of a given orientation that could be intersected if the borehole were drilled normal to each fracture plane.

3. Results

3.1. Core Description and Lithostratigraphy of TW4

Over 1150 ft of continuous core collected in TW4 from 646 to 1802 ft allowed for a detailed lithological description and unambiguous assessment of the vertical scope and relation of the sedimentary strata in the Palisade Sill contact zone, the marginal Stockton Formation, and the contact with crystalline basement (Figure 2). The first unit intersected by the test wells is the Palisade Sill made up of medium to fine-grained diabase (dolerite). In TW4, the main body of the sill extends to 691 ft below surface, followed by a ~6 ft-thick sheet of metasedimentary strata (691–697 ft), and a second finer-grained diabase section around 20 ft thick (697–717 ft). The metasedimentary rocks consist of dark gray mudstone hornfels and whitish sandstone (Figure 3a), which we interpret as a sedimentary xenolith. Such xenoliths are common in outcrops of the lower sill contact south of the study site, e.g., in North Bergen and Fort Lee, NJ (Figure 3b) [*Van Houten*, 1969; *Merguerian and Sanders*, 1995]. Below the lowermost section of the sill, the upper 20 ft have mudstones that are sufficiently altered to be called a hornfels [e.g., *Van Houten*, 1969] and the underlying arkosic sandstones, which are white to tan, sometimes with a pinkish (rosy) cast, are visibly metamorphosed for another ~30 ft. The mudstone hornfels from 717 to around 728 ft are dark gray and resemble the Lockatong Formation hornfels, similar to those observed in outcrops to the south below the Palisade Sill, e.g., in Alpine, NJ and Fort Lee, NJ, and parts of Rockland County, NY [e.g., *Olsen*, 1980; *Olsen and Rainforth*, 2001; *Yager and Ratcliffe*, 2010]. Because of the alteration due to the sill and the complexity of the lateral change in facies, this lithostratigraphic identification is not certain. Here we use the classical lithostratigraphic

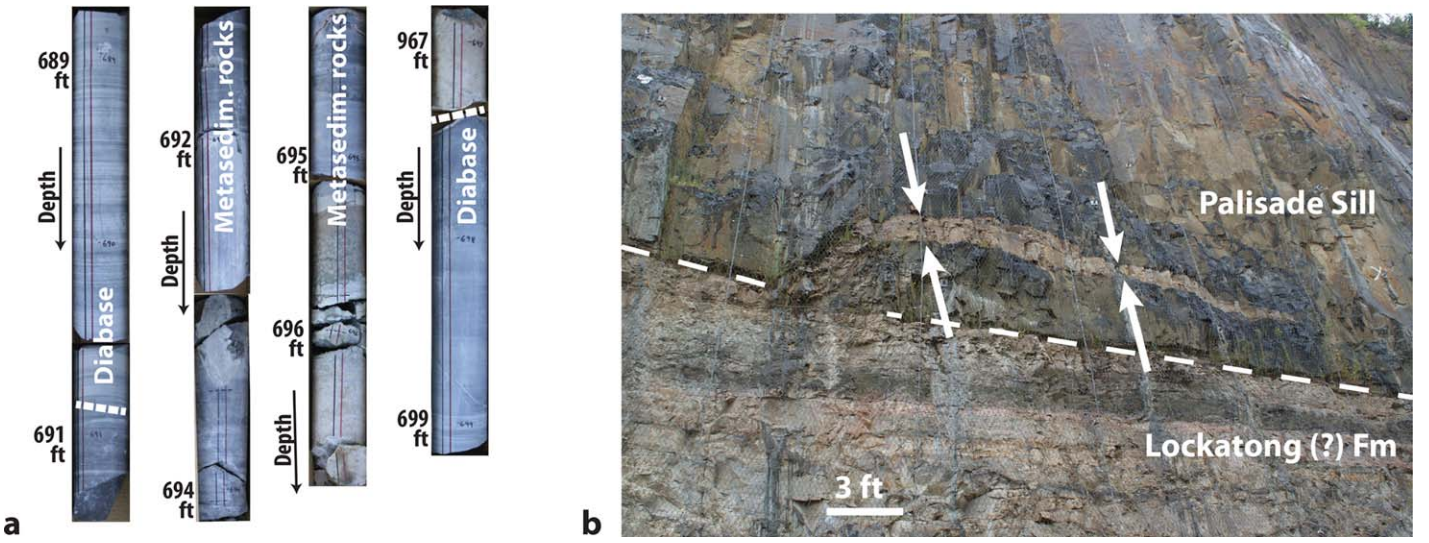

Figure 3. Sedimentary xenolith in the Palisade Sill contact zone. (a) Sedimentary strata trapped in diabase at the bottom of the Palisade Sill in TW4 core. A close examination allows distinguishing finely crystalline diabase from the hornfels mudstone of the Lockatong Formation. (b) a sedimentary xenolith inside diabase in an outcrop of the Palisade Sill's basal contact at 7101 River Rd, North Bergen, NJ (40 47 37.889°N, 73 59 53.051°W).

definitions of the three lowest and thickest formations in the Newark Basin [*Kümmel*, 1897, 1898, 1899; *Van Houten*, 1969; modified by *Olsen et al*., 1996; *Olsen*, 1980; *Smoot*, 1991], which are based on color and grain size of the dominant sedimentary strata and relation to each other (Table 1).

The sedimentary sequence from 756 to 1550 ft in TW4 consists of light-colored arkosic sandstones and conglomeritic sandstones alternating with red to purple mudstones (Figure 2). Mudstone color changes with depth from predominantly purple at the shallower depths to red, dark red, and dark purple in the deeper intervals. Significant lithological variations occur at the scale of meters to tens of cm. Most of the mudstones have very little observable bedding, are massive, have large desiccation cracks filled with sandstone to gravelly sandstone, and exhibit abundant features consistent with significant pedogenic modification, such as pedogenic slikensides, pedogenic-type nodules, root traces, and vague burrows [cf. *Smoot*, 2010]. Arkose sandstones are mostly tan and pink, and many appear to have vuggy porosity. A distinctly different section with thick layers of white conglomeratic sandstones separated by minor red-purple mudstones was encountered between 1086 ft and 1168 ft. X-ray diffraction (XRD) mineralogical analysis of half a dozen plugs from the sedimentary section indicated that clay content varies from ∼10% in sandstones to up to 70% in mudstones, and the clays predominantly consist of illite and mica [e.g., *Slater et al*., 2012]. In the Newark Basin lithostratigraphy, intervals of light-colored arkosic sandstones and conglomeritic sandstones alternating with red to purple mudstones low in the section are traditionally classified as the Stockton Formation [*Olsen et al*., 1996; *Olsen*, 1980; *Smoot*, 1991]. Therefore, this term is applied here to the interval from 756 to 1550 ft. It's important to note, however, that the expression of the Stockton Formation in TW4 and in outcrops along the Hudson River differ from the expression of the formation in its type area in the central Newark basin in having sandstone and mudstone intervals that are much thinner. Moreover, the Lockatong Formation clearly grades laterally into these facies, and thus it is possible that much if not all of what is lithologically identified as Stockton Formation in TW4 core could be the lateral equivalent of the Lockatong Formation. Given the predominance of arkosic sandstones and conglomerates typically attributed to the Stockton Formation however, we classify this part of the TW4 section as the Stockton (Table 1).

From 1550 ft to the contact with crystalline basement at about 1711 ft, the TW4 core is composed of mudstones and sandstones that form a sequence lithologically distinct from the rest of the overlying Stockton Formation, particularly for the upper and basal intervals (Figures 2 and 4). The upper part (∼1550–1590 ft) contains many thin sandstones that are fine-grained and become gradually coarser downhole. The sandstones are interbedded with mudstones that are often brick-red as opposed to the darker purple-red mudstones above them (Figure 4b). In addition, fractures in this interval are common and filled with fibrous

Table 1. Lithostratigraphic Basis of the Newark Basin Formation Identification

	Characteristic Formation Lithology Observed in TW4 Core	Deviations From the Standard Formation Definitions
Lockatong Formation	Alternating dark grey hornfels and white to tan arkosic sandstone	No lacustrine cycles could be identified in the short section below the sill
Stockton Formation	Light-colored arkosic sandstones and conglomeritic sandstones alternating with red to purple mudstones	Much smaller thickness of all strata than at the type localities

gypsum that may have had its origin in the mudstones themselves as described by *El-Tabakh et al*. [1997]. The basal part of the sequence (~1700–1710 ft) is a dark purple-brown mudstone that has intensely developed apparent pedogenic features, especially intense soil slikesides, rhizolitic (root) mottling and is unlike any unit described so far in the Newark Basin (Figure 4c). At its contact with the underlying gneiss, a thin gravelly sandstone forms a sharp contact with reddish basement at 1710.5 ft. The age of this unit is unknown; it is hypothesized to be Triassic in age, but could be as old as Late Permian. The dark purple-brown mudstone is hydrophilic, and swelled soon after drilling forming a bridge that prevented the logging tools from descending into the basement interval.

Crystalline basement in TW4 was encountered at a depth of 1710.51 ft. It is composed of granulitic gray gneiss, similar in appearance to the Fordham gneiss outcropping across the Hudson River in The Bronx, NY, and Westchester County, NY [e.g., *Abdel-Monem and Kulp*, 1968; *Isler et al*., 2009]. The upper 25 ft of the gneiss (1710.5–1736 ft) is mottled purple and pink that transitions into gray gneiss with fractures that are reddened at the edges. We interpret the reddened part as a paleo-weathered interval, with paleo-ground water alteration playing at least some role.

3.2. Core Physical Properties and Core-Log Integration in TW4

Continuous measurements of bulk density (ρ_b) and magnetic susceptibility (MS) on core allow a direct correlation of these petrophysical properties to core lithology. Each of the main three sections of the core—the Palisade Sill diabase, the sandstones and mudstones of the Stockton Formation, and the basement Fordham gneiss—are characterized by distinct ranges of these physical properties (Figures 4a and 5). The diabase is characterized by very high density (2.9–3.2 g/cm^3) and MS values (~10^{-2}–10^{-1} SI). The metamorphic basement has lower ρ_b but comparable MS values with two distinct clusters for weathered and unaltered gneiss (Figure 5a). The bulk density increases gradually from around 2.6 g/cm^3 in the weathered interval at 1711–1730 ft to around 2.80 g/cm^3 at 1775 ft, and remains at 2.75–2.78 g/cm^3, on average, at greater depths to TD (Figure 4a). Core magnetic susceptibly of the gneiss is relatively low–at the order of 10^{-4}–10^{-2} SI—in weathered gneiss, overlapping with the sedimentary range; but it increases sharply by at least an order of magnitude at the transition to unaltered gneiss at ~1736 ft to 10^{-3}–10^{-1} SI (Figure 4). In the sedimentary section, the physical properties reflect lithological variation of alternating sandstone and mudstone strata. Both ρ_b and MS have higher values in the mudstones (2.60–2.90 g/cm^3 and 10^{-4}–10^{-3}, respectively) and lower values in sandstones (2.30–2.60 g/cm^3 and 10^{-6}–10^{-4} SI, respectively). This pattern of alternating high and low values related to sandstone and mudstone strata is very consistent over a 700 ft-long depth interval from ~800 to ~1,500 ft. Only in a very narrow interval at the sill contact zone (~715–750 ft) this pattern is complicated by the sill's metamorphic overprint resulting in very high MS and density values in hornfels, comparable to those in diabase (Figures 4a and 5a). Outside of the contact-metamorphozed zone, the physical properties correlate well with lithology, and can be used for lithological classification within the Stockton Formation at this site.

The lithologically distinct section at the bottom of the Stockton Formation (1550–1711 ft) is characterized by slightly different physical properties than the 800 ft of sedimentary strata above it (Figure 4a). Both density and magnetic susceptibility of the core have smaller variability range and slightly higher average values than the strata above. A singular GR anomaly occurs within this interval at ~1594 m with total GR value an order of magnitude higher than elsewhere in the section (detected in the total GR downhole log, and verified with total and spectral GR measurements on core) (Figures 4a and 6). A high-resolution measurement of the total gamma ray activity of the core reveals four separate peaks within 4 ft depth interval at 1592–1596 ft (Figure 6). Spectral analysis indicated that most of the gamma activity at peak values is produced by bismuth (^{214}Bi), a uranium daughter product. Outside the peaks, gamma counts are low and the only

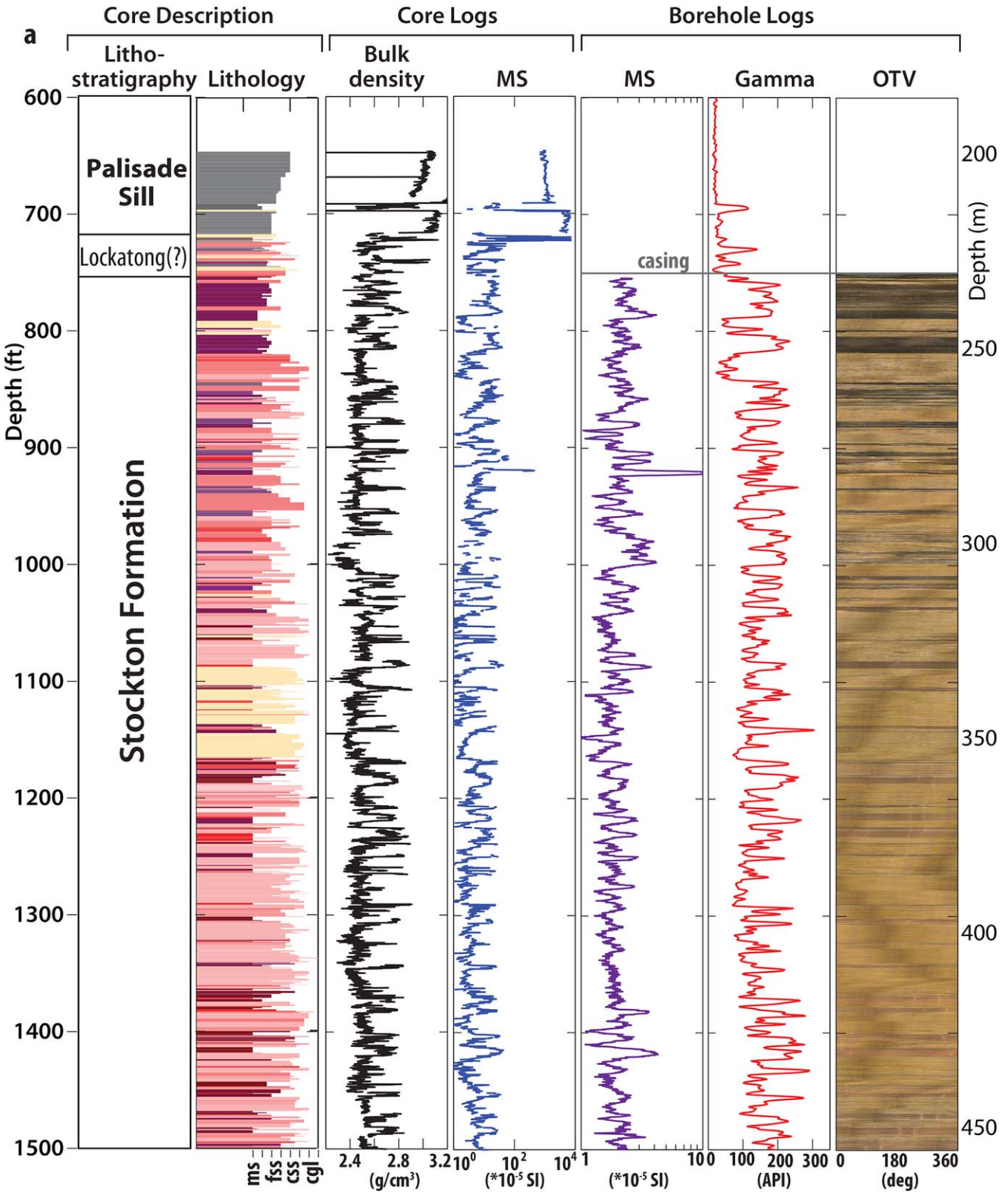

Figure 4. Core and logging data from TW4: (a) lithological description of the core and core-based lithostratigraphy (grain size notation: ms—mudstone, fss—fine sandstone, css—coarse sandstone, cgl—conglomerate; color corresponds to approximate RGB description of the core strata), bulkdensity and magnetic susceptibility (MS) measured on core, and borehole MS, total gamma and optical televiewer (OTV) logs; photographs of unusual intervals in the bottom section of TW4 core: illustrates (b) orange hue observed in the depth interval 1550–1620 ft; (c) the contact with the crytalline basement showing a dark purple-brown mudstone unlike any strata described in the Newark basin, followed by a sandstone-to-gravel layer overlaying reddened basement contact at 1711.5 ft. (The core boxes in the photographs are 3 ft long, cores are marked every foot the depth increases from left to right and bottom to top.)

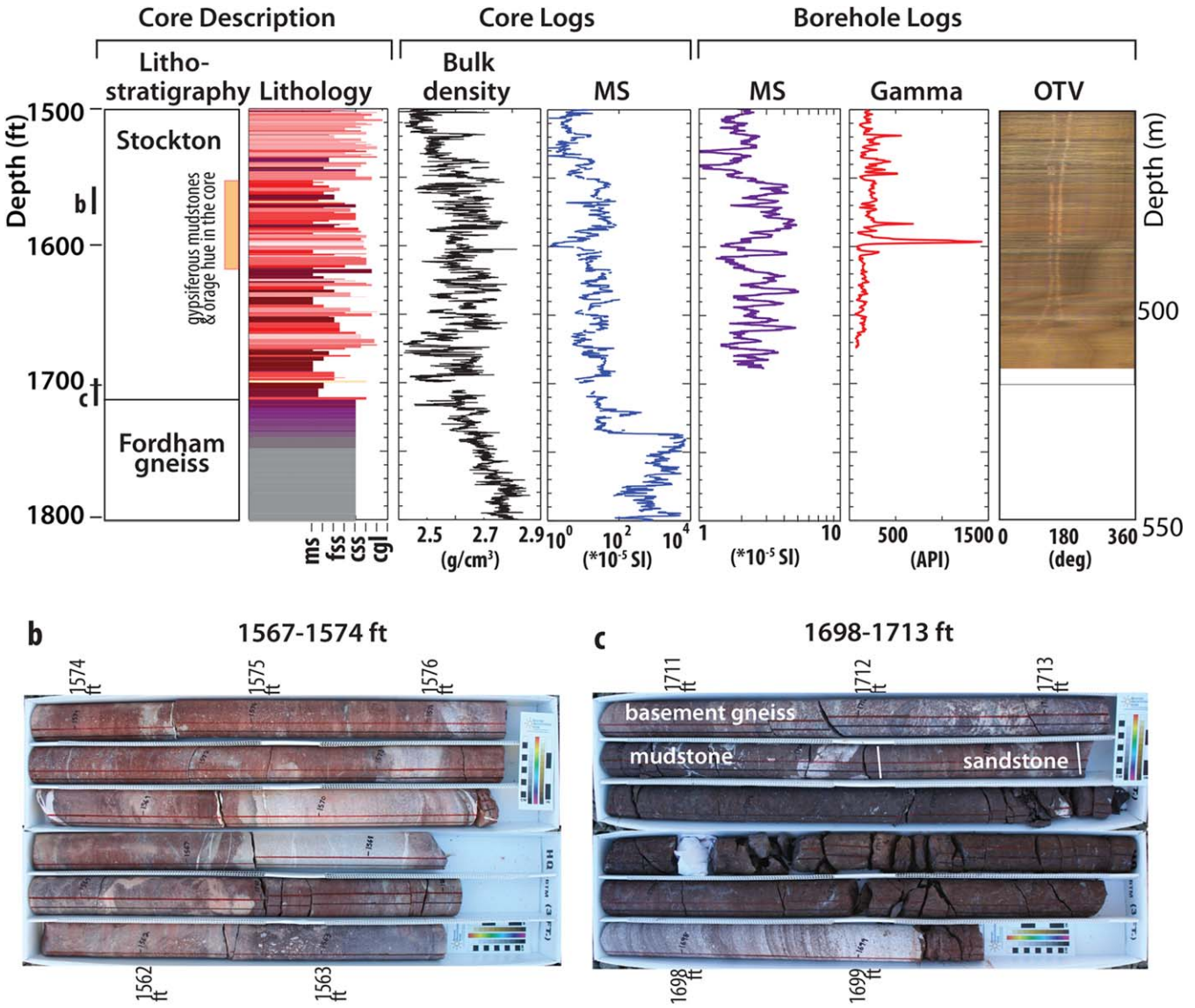

Figure 4. (continued)

distinguishable peak is produced by potassium (^{40}K), a common element in arkosic sandstones (Figure 6). As explained in the method section, detection of ^{214}Bi is a direct indicator of the uranium presence in the core. Therefore, the anomalously high gamma activity at 1592–1596 ft is attributed to elevated uranium concentration in this depth interval. This observation is very unusual as all other known instances of high uranium concentrations in the Newark Basin were found in black lacustrine mudstones of the Lockatong Formation and gray and black marginal-lacustrine sandstones of the Stockton Formation [*Turner-Peterson*, 1980], and have been related to black organic-rich mudstones and associated sandstone units. In the TW4 core, there are no back mudstones, and the uranium anomaly occurs in a dark-red sandstone with light-colored clasts (Figure 6).

In addition to a direct comparison between core lithology and physical properties, the core logs also allow for establishing accurate ties between core properties and borehole logs. In particular, magnetic susceptibility, measured independently at both scales (core and borehole), was very useful for this purpose. The borehole log (acquired only in the open-hole sedimentary section) has lower sensitivity and has much lower values than the core log, but the pattern of relative changes for different lithology is very similar—mudstones are characterized by higher MS values than sandstones in both core and borehole logs (Figures 5a–5c). The correlation coefficient between the core and downhole MS is 0.83, demonstrating an excellent

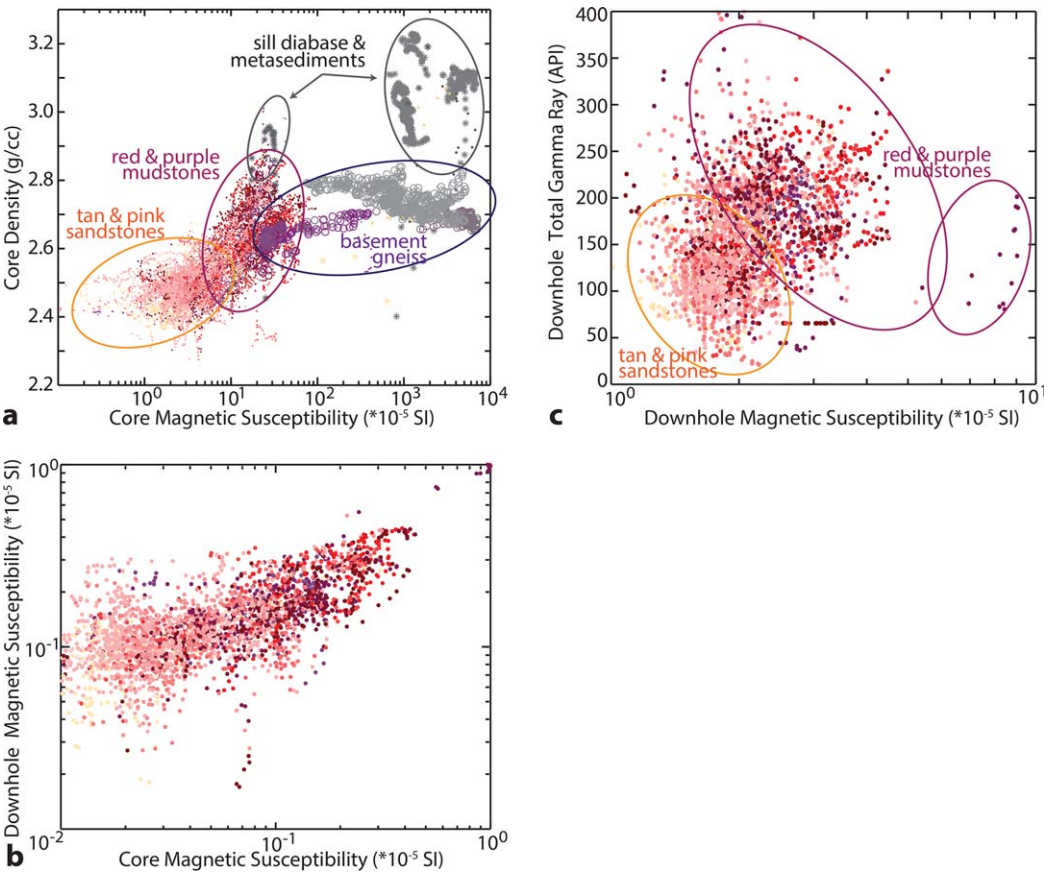

Figure 5. Petrophysical formation properties from TW4 core and log data: (a) a crossplot of core magnetic susceptibility and bulk density showing clustering in characteristic ranges for different lithologies; (b) a crossplot of core and downhole magnetic susceptibility normalized to [0, 1] range highlights some differences in the dynamic ranges but shows a close correlation between core and downhole MS (linear correlation coefficient of 0.83); (c) a crossplot of downhole magnetic susceptibility and total gamma ray activity shows more scatter than core data but discernible clusters for different lithologies. All points are color-coded based on corresponding core color on the same scale as litho-columns in other figures.

match of the measurements collected at both core and borehole scales. In turn, other downhole logs available in TW4 show a good match to MS and core lithology (Figures 4a and 5c). Despite some scatter present in the borehole data, light-colored (tan and pink) sandstone strata are characterized by low total GR and MS values, while darker-colored (red and purple) mudstones correspond to higher GR and MS values (Figure 5c). Optical televiewer image also allows clear delineation of the strata by different colors, which match exactly with the corresponding peaks and troughs in the GR and MS logs, and the core-based litho-column (Figure 4a).

The close correlation between core and downhole measurements demonstrates that downhole data can be reliably used for lithological and petrophysical description of the formation where gaps in the core data exist and/or where core was not collected at all, such as TW3. In TW4, only one interval of highly fractured core occurred at 985–1000 ft precluding reliable measurements of core physical properties (Figure 4a). The borehole MS log provides data to fill this gap, and clearly indicates elevated MS values, which can be attributed to mineral alteration and precipitation related to the enhanced fracturing and groundwater flow in this interval.

3.3. Petrophysical Properties in TW3

In the absence of core, downhole logs and drill cutting information were used for formation characterization in TW3. The logs span the Palisade Sill, the contact zone, and the underlying Newark Basin sedimentary strata (Figure 7). The sill diabase is characterized by low GR values (10–40 API) and high MS values ((20–100)*10^{-5} SI). An earlier petrographic study of the drill cuttings by *Goldberg and Burgdorff* [2005]

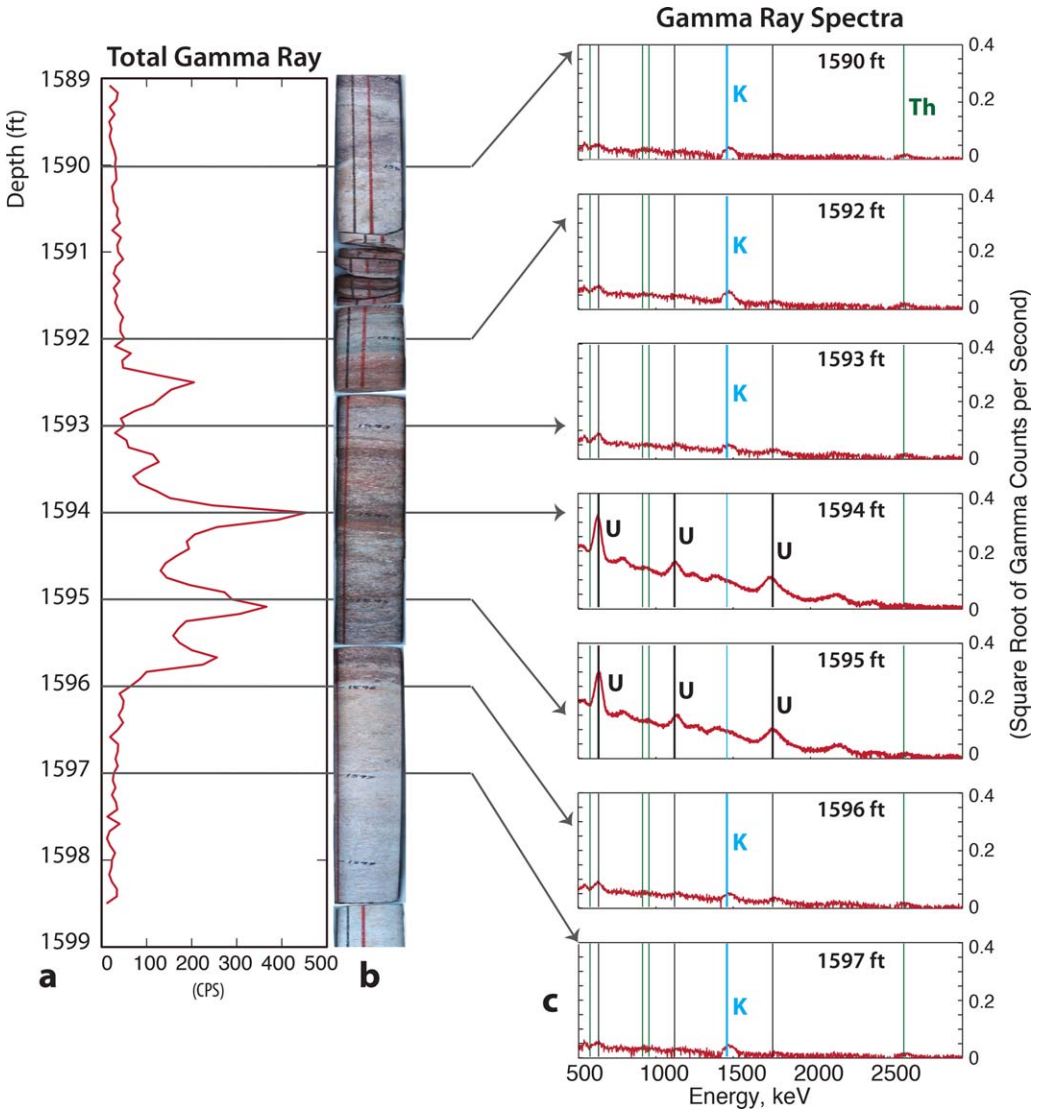

Figure 6. Spectral gamma measurements for the total gamma anomaly in TW4 indicative of a high uranium concentration. (a) high resolution total gamma ray measurement on the core reveal four narrow zones with high gamma counts at 1592.5, 1594, 1595.1 and 1595.8 ft; (b) the photographs of the core suggest a correlation of high gamma counts to dark-red oxidized zones; (c) gamma ray spectra are dominated by uranium peaks (identified by the daughter product ^{214}Bi at 609, 1120, and 1764 keV) at the depths of the highest total gamma counts, while the only noticeable peak in the low-intensity gamma spectra corresponds to ^{40}K (1461 keV).

identified compositionally distinct zones within the sill dominated by different pyroxene minerals (Figure 7). These mineralogical changes are not reflected in GR and MS logs. The contact between the Palisade Sill and underlying sedimentary strata is marked by sharp downhole increase in total gamma ray activity and pronounced changes of magnetic susceptibility, which fluctuates between very low values in light-colored sandstones and very high values in dark contact-metamorphosed mudstone hornfels and/or secondary layers of chilled diabase (Figure 7). Based on a stratigraphic projection from TW4 to TW3, and the similarity of appearance and physical properties, the metasedimentary strata below the sill are identified as the Lockatong Formation. A detailed comparison and lateral correlation of the contact zone between the two wells is provided in the Discussion section below.

In the sedimentary section below 850 ft identified as the Stockton Formation, downhole logs in TW3 exhibit a similar cyclical pattern to those in TW4, corresponding to alternating sandstone and mudstone strata (Figures 4a, 7, and 12). The GR log has a similar range to TW4: 50–100 API in sandstones and ~200 API in mudstones. The MS log has values of ~1–10 (*10^{-5} SI), also similar to TW4, but it is more attenuated in TW3

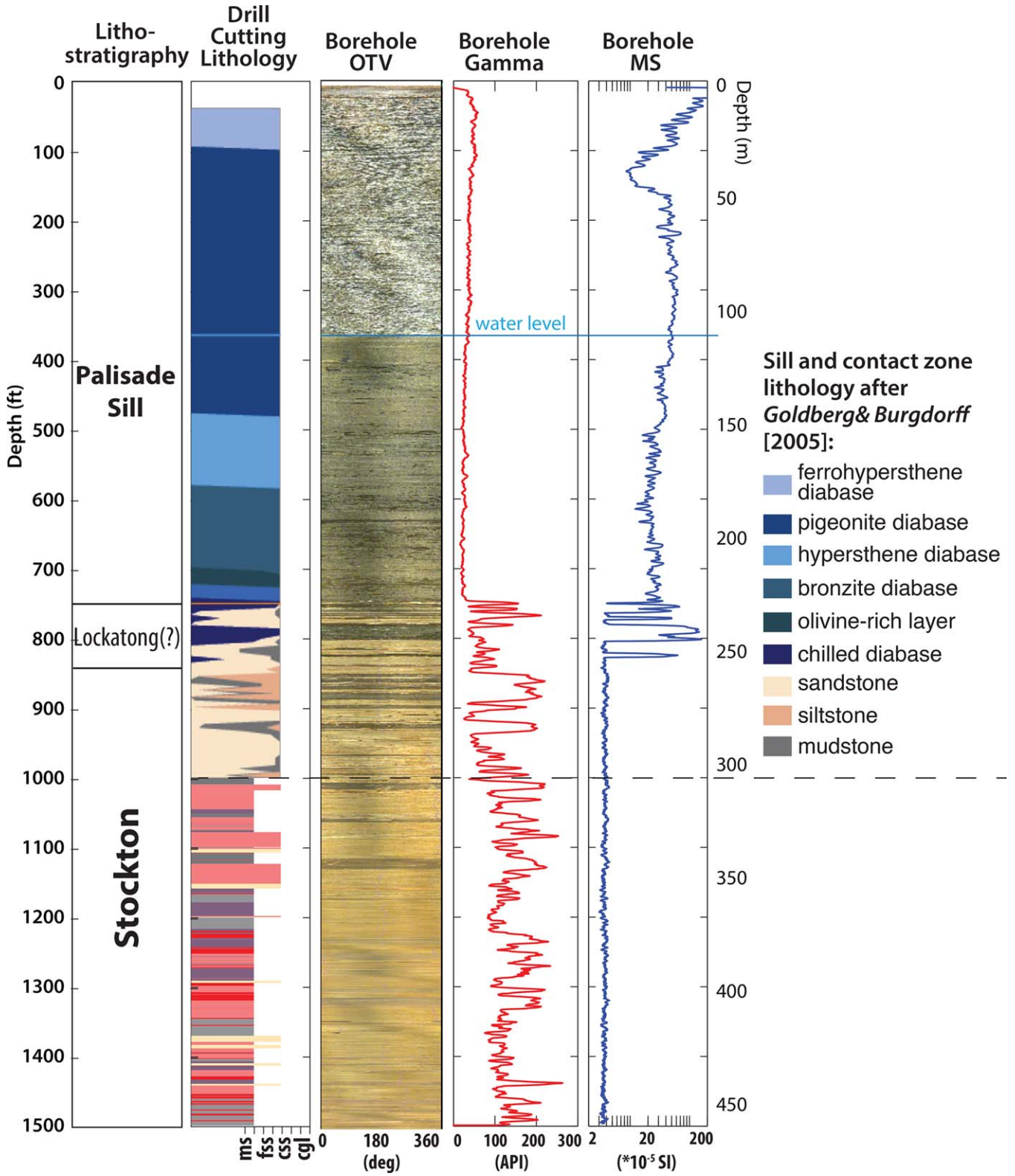

Figure 7. Downhole logging data and drill cutting-based stratigraphy for TW3. Drill cuttings lithology for 0–1000 ft is adopted from *Goldberg and Burgdorff*'s [2005] petrological description of thin sections, as indicated by the legend. For the bottom 500 ft, a dominant color (grey, pink, red, purple, tan) is plotted with a binary grain size classigication of either mudstone or sandstone after *Shao*'s [2011] cutting description (grain size scale is the same as in Figure 4). The borehole logs (optical televiewer (OTV), total gamma ray and magnetic suceptibilty (MS) were aquired as part of this study.

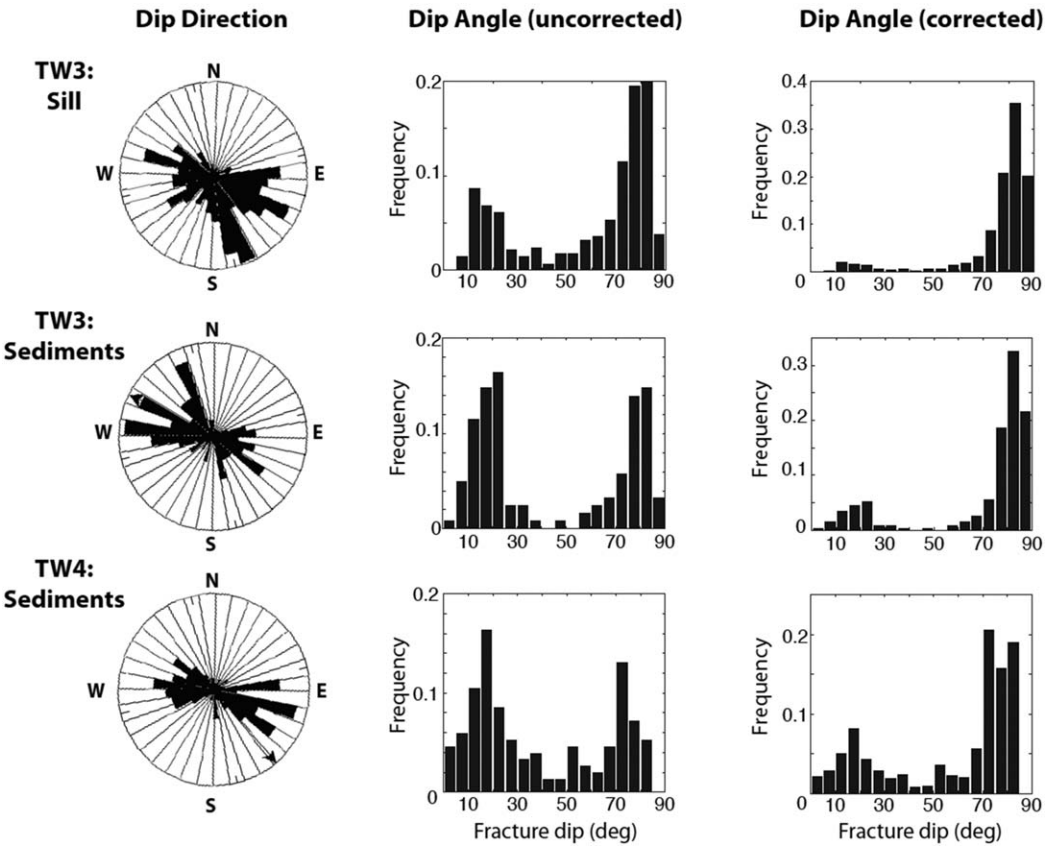

Figure 8. Fracture dip direction and dip angle based on borehole image analysis. Histograms on the right show fracture dips corrected for the systematic undersampling of steeply dipping fractures in vertical boreholes.

due to the larger hole diameter (Figure 12). A combination of physical properties, visual analysis of drill cuttings, and the optical televiewer log was used to interpret the lithostratigraphy encountered in TW3. Overall, TW3 is quite similar to TW4, dominated by tan and pink sandstones with thinner purple to red mudstone layers. However, a more detailed lithological analysis was not possible because of poor preservation of fine-grained material in the cuttings and a high degree of mixing of grains from different strata. A simplified litho-column is presented in Figure 7 using a binary grain size classification (mudstone/siltstone versus coarse sandstone) and a single dominant color reported by *Shao* [2011].

3.4. Fractures and Hydraulic Properties in TW3 and TW4

Observations of TW4 core and borehole televiewer data reveal abundant fractures both in the Palisade Sill and the Newark basin sedimentary strata. Most of the fractures fall in two broad sets: low angle fractures dipping to W-NW, and high angle fractures dipping to SE, with some variability in dip direction and fracture density (Figures 8–10). These two fracture sets are consistent with previous observations and tectonic history of the basin [*Heisig*, 2011; *Herman*, 2009; *Matter et al*., 2006; *Goldberg and Burgdorff*, 2005; *Goldberg et al*., 2003; *Morin et al*., 1997]. Four main subsets were observed in the Palisade Sill in TW3: subvertical sets that dip E, SE, and SSE, and a shallow-angle set dipping NW (Figure 8). The sill is densely fractured, with intervals of massive diabase less than 10 ft thick (Figure 9c). Observed features represent a combination of basalt cooling joints and tectonic fractures formed after the sill emplacement. Shallow-angle fractures are dominant in the shallower part of the sill (above 650 ft), related to unloading and lower vertical stresses at shallow depth. High-angle fractures striking NE-SW dominate in the bottom part of the sill, and in the sedimentary strata close to the sill contact (Figure 9c). Deeper in the sedimentary section the shallow-dipping fractures are more common than high-angle fractures. When corrected for sampling bias, the histograms of fracture dip in TW3 and TW4 retain the bimodal pattern but suggest much higher frequency of steeply dipping fractures (Figure 8). This sampling bias correction assumes uniform fracture spacing and does not

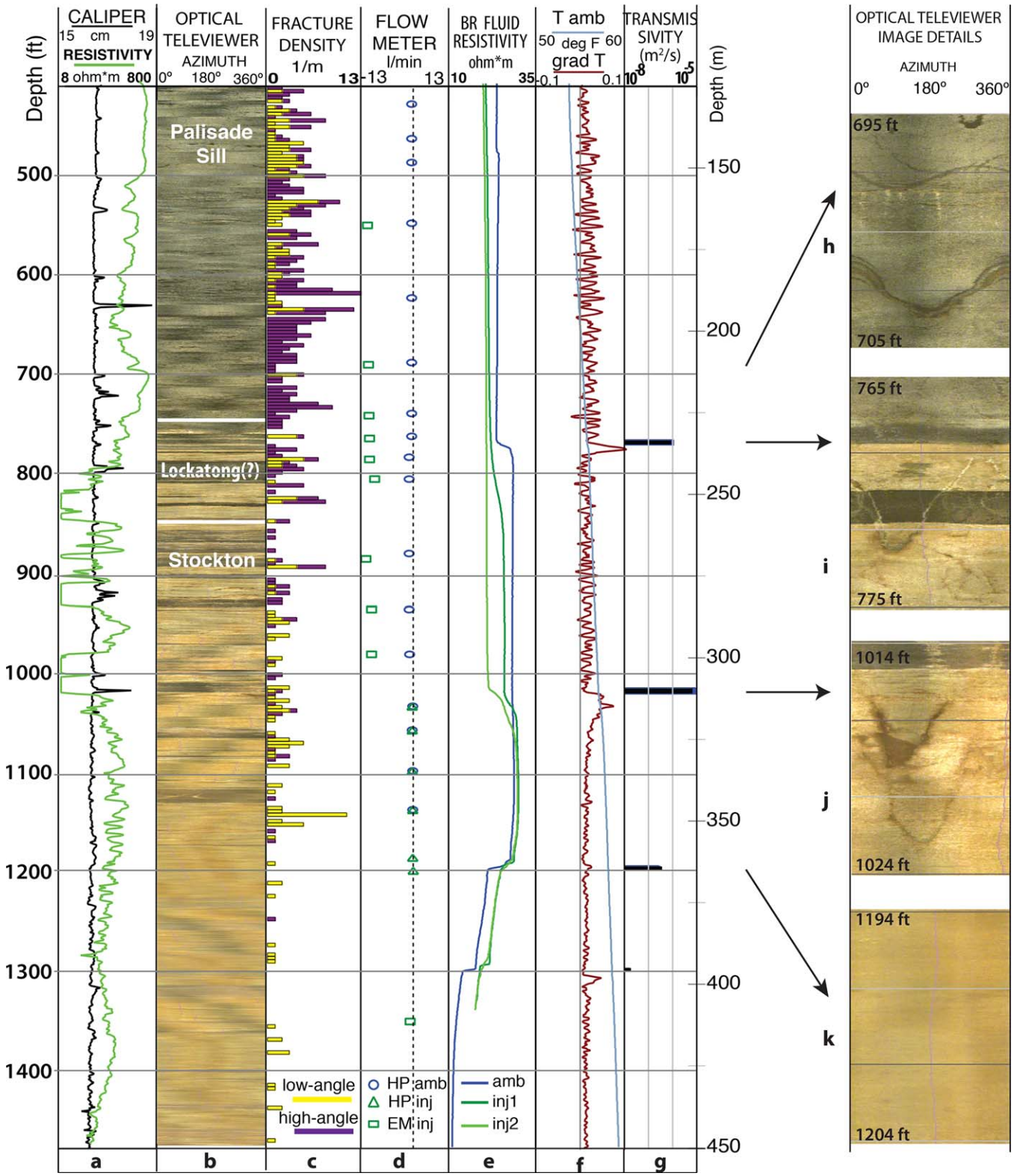

Figure 9. Summary of hydraulic testing results in TW3. (a) Hole diameter (caliper) and electrical resistivity logs, (b) optical televiewer image; (c) density of fractures identified in televeiwer images (yellow for low-angle, purple for high angle dip); (d) vertical flowmeter data: ambient (amb) in blue, during injection (inj) in green, EM—electromagnetic, HP—heatpulse; (e) borehole fluid resistivity: ambient (amb) in blue, two consecutive measurements during injection (inj) in green; (f) borehole ambient temperature (T amb, blue) and temperature gradient (grad T, red) logs; (g) transmissivity estimated from borehole hydraulic testing (black), (h) an example of nontransmissive fractures in the Palisade Sill as seen in the televiewer image; (i, k) details of the televiewer images in transmissive intervals: Figures 9i and 9k correspond to distinct steeply dipping fractures, deeper intervals correspond to shallow-dipping fractures and/or primary porosity, and lack of visible features in the televiewer image.

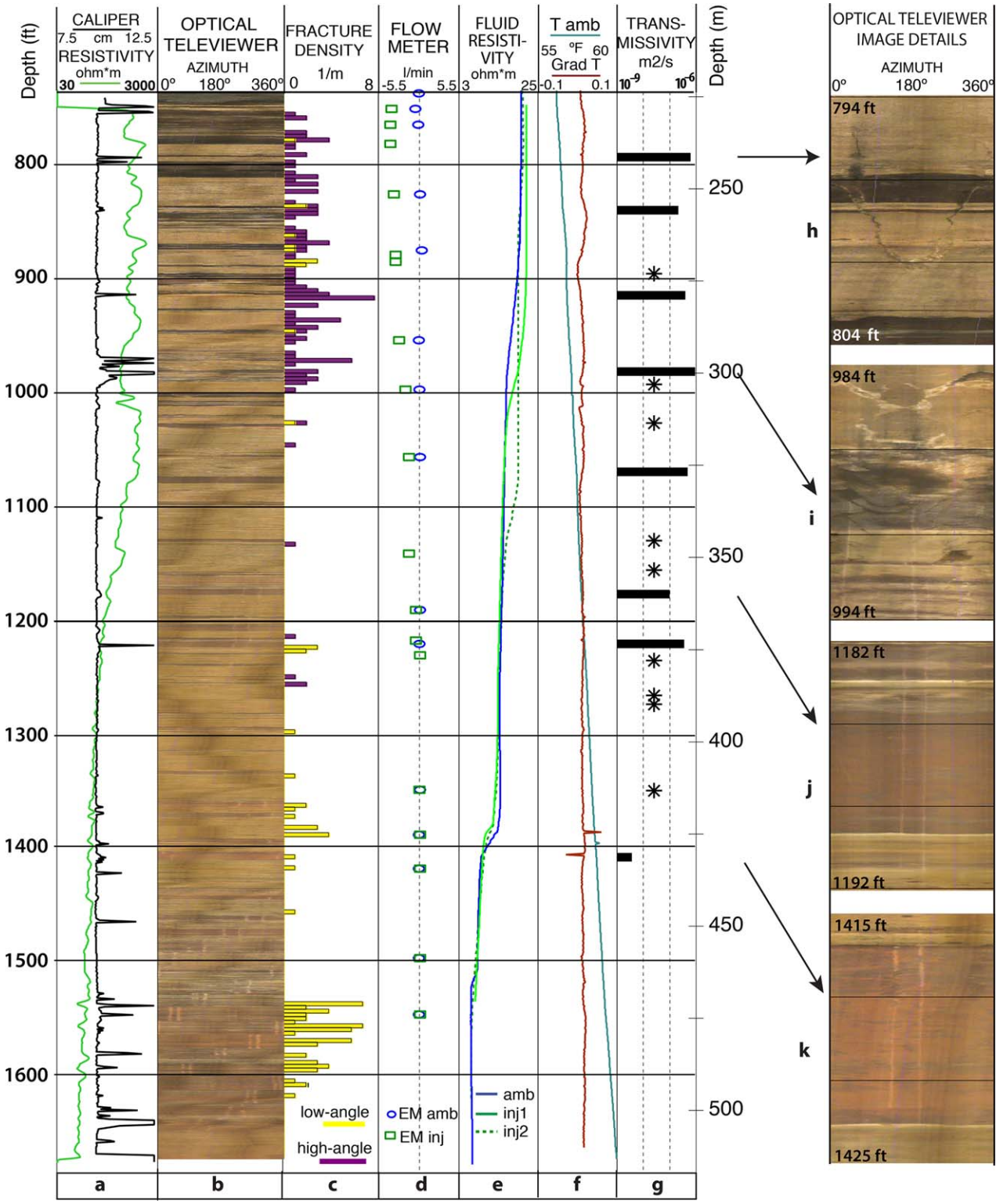

Figure 10. Summary of hydraulic testing results in TW4. (a) Hole diameter (caliper) and electrical resistivity logs; (b) optical televiewer image; (c) density of fractures identified in televeiwer image (yellow for low-angle, purple for high angle dip); (d) vertical electromagnetic (EM) flowmeter data: ambient in blue, during the injection in green; (e) borehole fluid resistivity: ambient in blue, two consecutive measurements during injection in green; (f) borehole ambient temperature (T amb, blue), and temperature gradient (grad T, red) logs; (g) transmissivity estimated from borehole hydraulic testing; stars indicate sampling depths for laboratory porosity and permeability measurements, which yielded helium porosity of 10–17% and air permeability of 1–20 mD [*Slater et al*., 2012]; (h–k) details of the televiewer images in transmissive intervals: shallow transmissive intervals correspond to distinct steeply dipping fractures, deeper intervals correspond to shallow-dipping fractures and/or primary porosity.

account for local variations in fracture spacing. Therefore, the corrected abundances likely overemphasize the steeply dipping fractures, and the true distributions of fracture dips lie in between the two cases illustrated in Figure 8.

Hydraulic testing in the TW3 and TW4 boreholes indicates that transmissive zones in the Stockton Formation below the Palisade Sill are sparse, narrow, and characterized by low, if any, ambient flow (Figures 9 and 10). Only four hydraulically conductive zones were detected in TW3 during an injection test: at the depths of 770 ft, 1010 ft, 1200 ft, and 1300 ft. These depths are marked by changes in borehole fluid resistance, fluid temperature and flow rate under both ambient and injection conditions (Figures 9d–9g). The upper zone at 770 ft coincided with the previously identified conductive region in the sill-sediments contact zone [*Matter et al.*, 2006]. Despite pronounced resistivity changes, the ambient fluid flow at the two deeper zones at 1200 ft and 1300 ft was below detection limit of the flowmeters (0–0.1 L/min). The most conductive zone at 1010 ft had an ambient flow rate of about 1 L/min. Based on the injection test, the transmissivity of this zone was estimated to approach 10^{-5} m^2/s. The least conductive zone at 1300 ft was characterized by a transmissivity of $\sim 10^{-8}$ m^2/s (Figure 9g). The two upper zones with higher transmissivity values correspond to prominent high-aperture high-angle fractures observed in the OTV images (Figures 9h–9i). The lower zones do not exhibit any fractures in the borehole (Figure 9j), and are likely characterized by a combination of primary and secondary porosity. The Palisade Sill and low-permeability sedimentary strata separating these zones exhibit zero transmissivity.

In TW4, eight conductive zones were identified, with transmissivities on the order of 10^{-9}–10^{-6} m^2/s (Figure 10). No ambient flow was detected in any of these zones. The upper four transmissive zones correspond to prominent high-angle fractures, and the bottom four to low-angle or no visible fractures in the borehole images and core (Figures 12h–12k). The interval with highest transmissivity (10^{-6} m^2/s) at 990 ft coincides with the single most fractured zone that was marked by the recovery of rubbled core and enlarged borehole size (Figure 10a). Only select transmissive zones correspond to changes in borehole fluid resistivity and temperature gradient (Figures 10e–10g). Due to a relatively sparse spacing of flowmeter measurements, the exact depth and thickness of these conductive zones is not well constrained. Overall, the distribution of hydraulically conductive zones in TW4 is different from that in TW3, with a larger number of less conductive intervals, and most of those occurring at shallower depths.

4. Discussion

4.1. New Insights into Geology of the Northeastern Newark Basin and Lateral Extent of Lithological Units

The close proximity of the TW3 and TW4 boreholes allows evaluating the spatial extent of individual structural and lithological features identified in log and core data. TW3 is located 700 ft away from TW4 in a roughly downdip direction, with an average bedding dip of ~9 degrees. Therefore, the hole or core depth offset between the same strata is projected to be about 100 ft (i.e., if laterally continuous, the same features should occur 100 ft deeper in TW3 than in TW4). TW3 did not reach the contact with the crystalline basement; thus, neither the basement surface dip nor the extent of the uranium anomaly in the strata above basement could be evaluated. However, the Palisade Sill contact zone and the majority of the underlying Stockton Formation are represented in both boreholes, and their expression can be compared to constrain lateral variability of formation units.

Comparison of the Palisade Sill contact zone in the two wells illustrates the structural complexity of the sill intrusion path. The TW4 core allowed unambiguous identification of a sedimentary xenolith at the bottom of the Palisade Sill at 691–697 ft, and the contact with the Lockatong Formation at 717 ft (Figure 11). Logging data in TW3 indicate the occurrence of sedimentary rocks at a depth of 746 ft, but it is not clear whether any of the subsequent dark strata with low GR and high MS values correspond to secondary diabase bodies or the hornfels (Figure 4). Prior studies that relied on logging and drill cuttings analysis suggested that multiple stringers of diabase might exist below the primary sill contact (Figure 7) [*Matter et al.*, 2006; *Goldberg and Burgdorff*, 2005]. The new analysis of TW4 core lithology and physical properties indicates that the hornfels cannot be reliably distinguished from diabase based on GR and MS values alone (Figures 4a and 5a). Moreover, multiple ($\geq$2) diabase bodies/sedimentary xenoliths have not been observed in the outcrops, and individual xenoliths seen in outcrops are not ubiquitous and do not extend for hundreds

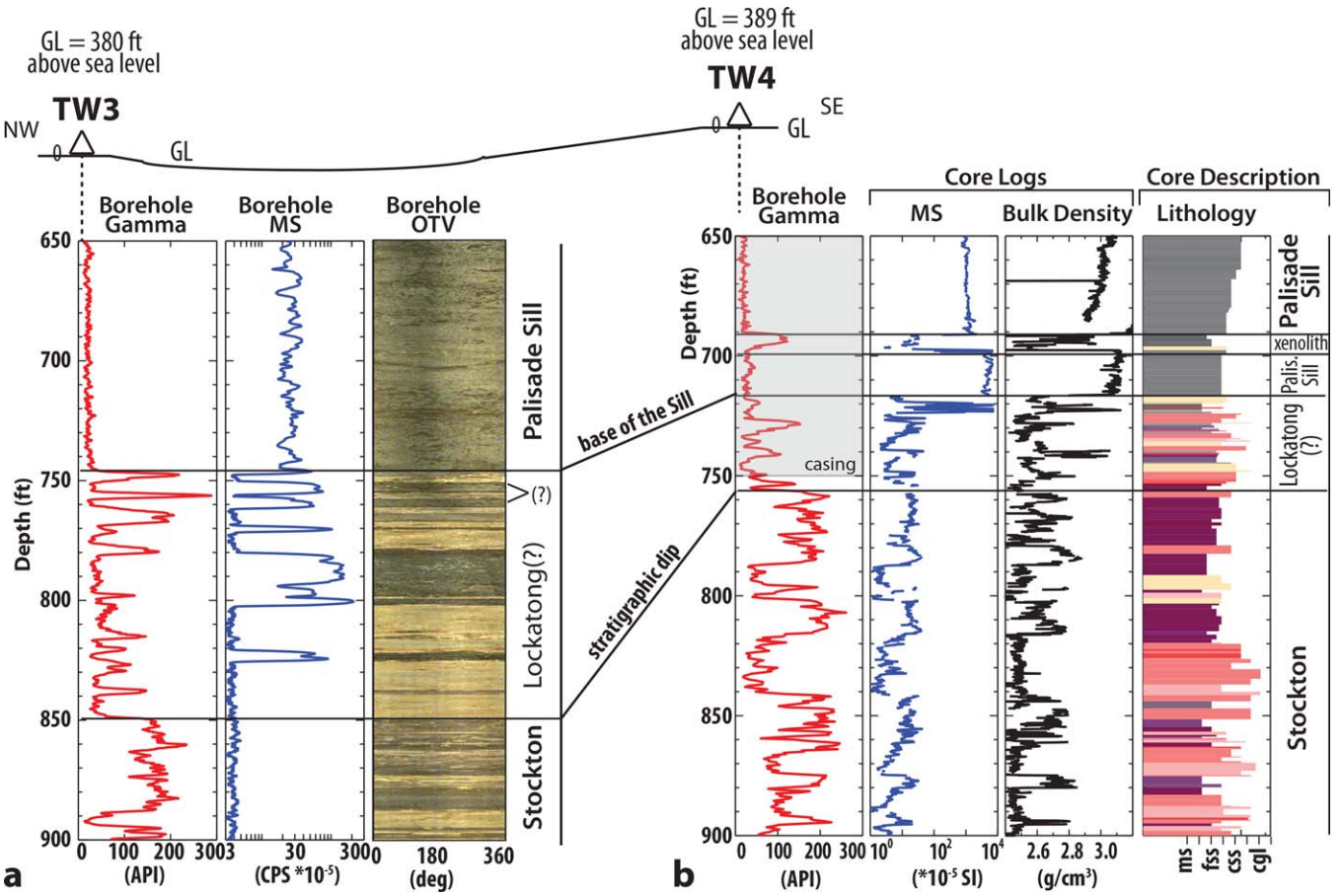

Figure 11. Lithostratigraphy and physical properties in the Palisade Sill contact zone. (a) Borehole logs in TW3 (gamma, magnetic susceptibility (MS), and optical televiewer image (OTV); (b) borehole gamma log and core measurements from TW4: core MS, core bulk density, and core lithology (ms—mudstone, fss—fine sandstone, css—conglomeritic sandstone, cgl—conglomerate). Core data in TW4 reveal a sedimentary screen at the bottom of the Palisade Sill. In TW3, unambiguous identification of the contact zone structure is not possible in the absence of core, but geophysical data suggest the sill contact occurs at a shallower stratigraphic level.

of feet (e.g., Figure 3b). We therefore conclude that there is not enough evidence to support the presence of multiple sedimentary xenoliths and/or diabase layers in TW3, and we consider the 746 ft boundary as the primary contact between diabase and underlying Lockatong strata. From this it follows that the depth offset of the Palisade Sill contact in the two wells is only 746–717=29 ft, and therefore, the sill does not strictly follow the sedimentary layering. At the studied location the sill appears to 'jump' across the stratigraphic section, consistent with other studies documenting the sill jumps in the region [e.g., *Olsen* 1980; *Goldberg and Burgdorff*, 2005; *Olsen*, 1980].

In the main section of the Stockton Formation penetrated by both boreholes, the downhole logs exhibit a similar cyclical pattern, corresponding to alternating sandstone and mudstone units (Figures 4a and 7), but no individual layers could be reliably traced from one hole to the other (Figure 12). Based on drill cuttings and optical televiewer data, the overall lithology in TW3 is similar to TW4, dominated by tan and pink sandstones with thinner purple to red mudstone layers, and the bedding statistics are nearly identical (Figures 12a and 12d). However, despite their close proximity and similar characteristics, one-to-one correlation of sedimentary sequences in these boreholes is not possible, suggesting significant small-scale variability in the depositional environment of these late-Triassic Newark basin sediments. Similar lateral variation in facies and unit thickness are visible in local outcrops near the study site [e.g., *Olsen and Rainforth*, 2001; *Savage*, 1968]. Although not unexpected near the basin edge, characterized by more diverse and dynamic depositional environment than in the center of the basin, this is an important direct observation of the small scale of lateral and vertical variability in the marginal Stockton facies. In contrast, core and outcrop studies in the central Newark basin identified regionally extensive lithostratigraphic units traced over many

kilometers of lateral distance [e.g., *Olsen et al*., 1996; *Kent et al*., 1995]. The distribution of the transmissive zones within TW3 and within TW4 is also quite different (Figures 9 and 10). Correspondingly, this suggests lateral heterogeneity in hydraulic, as well as lithological, properties of the Stockton Formation at the northeastern basin edge and is consistent with prior observations of the compartmentalized nature of shallow aquifers in Rockland County, NY, and limited east-west hydraulic continuity with dominant flow along the bedding strike direction, i.e., in NNE-SSW [*Heisig*, 2011].

An occurrence of elevated uranium concentration in TW4 core, although not traceable to TW3, warrants a discussion due to its anomalous lithological setting. Uranium deposits in siliciclastic rocks commonly occur either in organic-rich black shales deposited in reduced conditions [e.g., *Spirakis*, 1996] or at redox boundaries in sandstones, where it is precipitated from groundwater under reducing conditions caused by reducing agents such as abundant organic matter and sulphides [*Jensen*, 1958; *Hostetler and Garrels*, 1962]. In the Newark basin, high uranium concentrations have been reported in two facies: black lacustrine mudstones of the Lockatong Formation and gray and black marginal-lacustrine sandstones of the Stockton Formation [*Turner-Peterson*, 1980]. The lithology observed in the TW4 core intersecting the high-uranium zone is very different from other known types of uranium deposits in the basin. *Turner-Peterson* [1980] described uranium-containing Stockton sandstones as gray with pods of pyrite and light-gray clay clasts, and traced the source of uranium to layers of black mudstones occurring nearby. In the TW4 core, there are no back mudstones, and the uranium anomaly occurs in a dark-red sandstone (Figure 6) with light-colored clasts up to ~0.5 inch in diameter. There is, however, a single narrow zone of gray sandstone at 1592 ft, approximately 2.0 ft above the uranium-rich zone. It corresponds to low gamma counts and is only about a few inches thick, but it is unique in the TW4 core and suggests that unusual redox conditions might have existed at this depth. There is no visible pyrite in or around this anomalous zone. However, a larger depth interval in the TW4 core around the uranium anomaly, from ~1550 to 1610 ft, exhibits an unusual orange hue, which could indicate the presence of uranium compounds or jarosite and related solid solution minerals. The latter are hydrous sulfates of iron and potassium (or sodium in natrojarosite) with characteristic orange and yellow colors, which can be formed by oxidation of iron sulfates, and have been linked to uranium occurrence in oxidized sedimentary rocks [e.g., *Yilmaz*, 1981]. Moreover, this larger depth interval contains abundant fractures filled with fibrous gypsum (Figures 4a and 4b), which suggests that this interval may have experienced active groundwater flow in the past bringing dissolved uranium that was deposited at a redox boundary near ~ 1592 ft. It is not clear why the uranium anomaly is concentrated only within a narrow interval. The TW3 hole did not reach the corresponding stratigraphic level; therefore, the lateral extent of the anomaly is not known. It is also possible that high gamma ray counts are produced by a few 'foreign' clasts in the sandstone matrix, and thus, do not reflect redox conditions in this paleo-aquifer. More study sites and detailed geochemical analysis will be required to determine the lateral extent of the uranium anomaly and its origin.

4.2. Hydrogeological Setting at the Site in the Context of the Northern Newark Basin Hydrology

Shallow fractured-rock aquifers define the principal groundwater system in the Newark basin, and they have been extensively studied in the central part of the basin [*Lacombe and Burton*, 2010; *Morin et al*., 2000, 1997; *Houghton*, 1990] and in Rockland Couty, NY [*Heisig*, 2011]. Based on the analysis of hydraulic data from over 100 wells that penetrate to depths of up to 600 ft, three types of water-bearing features (WBFs) were identified: (1) bedding planes and layers, (2) tectonic fractures, and 3) linear intersection of bedding and fracture planes [*Herman*, 2010]. In this classification, Type 1 includes transmissive beds (densely fractures tabular units and beds containing mineral-dissolution zones within gypsum paleosoil horizons), and any features related to stratigraphic layering, e.g., bed partings. The bed partings, or bedding fractures, are defined as mechanical breaks along bed contacts of different properties, such as gray or black beds and massive red mudstones [*Herman*, 2010; *Michalski and Britton*, 1997]. They can form transmissive zones that extend laterally for hundreds of feet, but are more common in the Brunswick aquifer (in the Passaic, and younger formations) [*Herman*, 2010; *Morin et al*., 1997]. The WBFs of Type 2 correspond to any conductive fracture that are not bed-parallel, including steeply dipping extension fractures and gently dipping shear fractures. This is the dominant type of WBF in the basin, especially so in the diabase and Lockatong aquifers [*Herman*, 2010]. Type 3, which is the intersection of 1 and 2, is less common, but plays an important role for cross-aquifer transport. The overall hydrologic model for the Newark basin was described as a leaky, multiaquifer system [*Herman*, 2010; *Michalski and Britton*, 1997]. The Stockton is described as the most

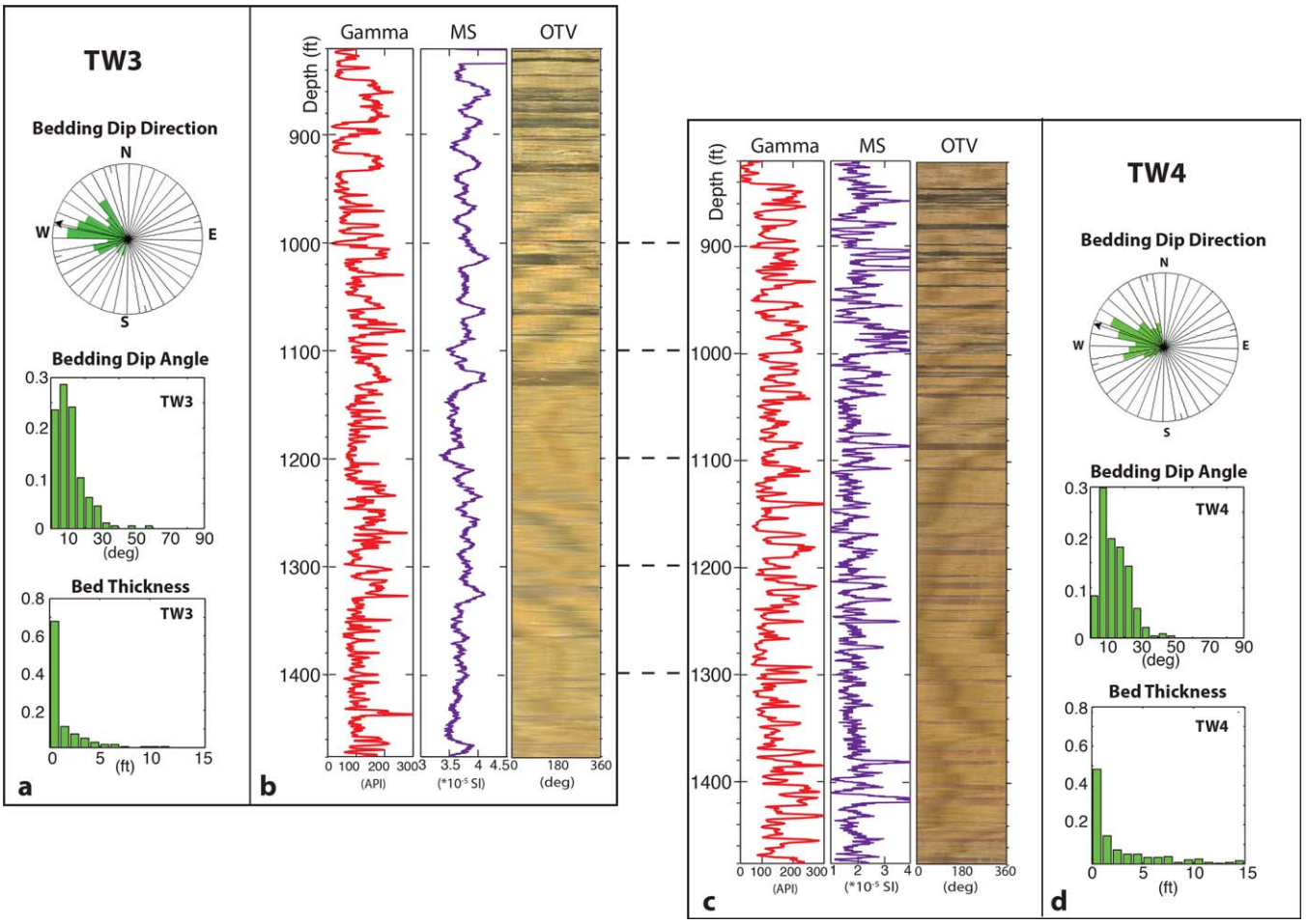

Figure 12. Lateral variability in the Stockton Formation. (a) Comparison of downhole data and bedding statistic from the two test holes (TW3 and TW4) located 700 ft apart. Logging data (b and c) are aligned to the same stratigraphic level computed with an average bedding dip of 9° to NWW, as measured in the optical televierwer images (OTV). Dashed lines represent the same stratigraphic levels. Bedding diagrams (a and d) summarize bedding statistics determined from OTV, and are very similar in the two wells. However, unambiguous layer-by-layer correlation of logging data in Figures 12b and 12c is not possible suggesting high lateral heterogeneity of the formation.

hydraulically conductive among Newark basin formations due to its many fractured beds and weathered arkosic sandstones [*Herman*, 2010]. However, water well yield data in the most northeastern part of the basin, although sparse in the Stockton Formation, indicate some of the lowest recorded in Rockland County, NY, and suggest an inferior hydraulic properties in shallow formations in the northeastern basin edge [*Heisig*, 2011].

The new hydraulic testing data from the Lamont wells constrain the properties of Newark basin aquifers at greater depths (~700–1700 ft) than the previous studies described above. The same types of WBFs were observed: bed-parallel fractures, partings and conductive layers, and steeply dipping tectonic fractures (Figures 8–10), but their abundance and trasmissivity is lower at the greater depths. In particular, the Stockton Formation, capable of water supply rates up to hundreds of gallons per minute (~10 L/s) at shallow depths in the central Newark basin, is significantly less transmissive in the studied interval. Transmissive zones with the Stockton Formation in TW3 yielded flow on the order of gallons per minute [*O'Mullan et al*., 2015; *Yang et al*., 2014]. The lower transmissivities observed here can be explained by a combination of two factors: 1) an increased overburden at greater depths, closing fractures and therefore reducing bulk conductivity, and 2) closer proximity to the basin edge where the Stockton Formation grades laterally into the Lockatong, which exhibits inferior hydraulic properties basin-wide [*Herman*, 2010]. Another distinction of the deeper aquifers in the Stockton at this locality is that some of the steeply dipping fractures are even more transmissive than bed-parallel features, while in shallow aquifers bedding fractures and bed-parallel

units were shown to exert primary controls on the groundwater flow [*Heisig*, 2011; *Herman*, 2010; *Morin et al*., 2000; *Michalski and Britton*, 1997]. This difference, however, may be caused by the proximity of these aquifers to the Palisade Sill intrusion path.

Steeply dipping fractures are clearly more abundant closer to the Palisade Sill contact than in the deeper strata below it (Figures 9c and 10c). The extent of this densely fractured interval, roughly 300 ft below the sill boundary in both boreholes, is consistent with the thermal and hydrofracturing effects induced by the sill emplacement and the depth extent of those effects on basin sedimentary strata. The rate of heating from an intrusion in the host formation scales with the distance from the contact and the permeability of the basin sedimentary rocks. As a rule of thumb, noticeable metamorphism is predicted to extend to a distance comparable to the intrusion thickness, while magmatic fluids penetrate only to the distance of ~1/3 of the intrusion size [*Hanson and Barton*, 1989; *Barton et al*., 1991; *Hanson*, 1995]. Fluid production from magma and the surrounding rocks is thought to be the dominant process responsible for hydrofracturing and subsequent thermal cracking within the intrusion contact zones [*Hanson*, 1995]. Pervasive fracturing in sedimentary strata for ~300 ft below the Palisade Sill contact is consistent with an average observed sill thickness of around 1000 ft [*Drake et al*., 1996]. Moreover, hydraulic fractures always open in the direction perpenticular to the minumum principal stress [*Hubbert and Willis*, 1957], which during the time of the Newark basin formation and the Palisade Sill emplacement was oriented NW-SE [*Goldberg et al*., 2003]. This favored the formation of subvertical extentional fractures that strike NE-SW in the current day basin sedimentary strata. Therefore, we conclude that intrusion of the Palisade Sill promoted formation of these steeply dipping fracures close to the sill contact.

An important question for understanding hydraulic setting in the basin is whether enhanced fracturing below the Palisade Sill contact also entails higher formation transmissivity along intrusion boundary compared to unaffected sedimentary strata. Existing data in TW3 and TW4 does not provide an unambiguous answer. On one hand, the majority of steeply dipping fractures observed in both boreholes are not hydraulically conductive at the present (Figures 11 and 12). On the other hand, of those steeply dipping fractures that are conductive, some have the highest transmissivities encountered in both boreholes. This suggests a possible correlation between the most permeable intervals and the intrusion path of the Palisade Sill [e.g, *Matter et al*., 2006], but it cannot be unambiguously proven with the existing data. More hydraulic tests are needed at different depths near the intrusion boundary and at other locations to establish such a correlation.

4.3. Implications for Assessing CO_2 Storage Potential in the Newark Basin and Other North American Rift Basins

The new cores and borehole data collected in the northeastern Newark basin confirmed that coarse sandstones are a dominant lithologic component at this basin edge, but borehole hydraulic tests indicated that they do not have sufficiently thick and permeable zones to accommodate large-scale fluid injection (Figures 9 and 10). Cross-well analysis also showed that most sandstone units and individual transmissive intervals are not laterally extensive, and the majority of fractures at depth are closed and do not transmit fluids. No significant matrix permeability was detected in borehole tests in the majority of the sandstone strata. These field-scale observations differ from the centimeter-scale laboratory analysis of sandstone permeability in TW4 core [*Slater et al*., 2012]. The laboratory measurements on 10 sandstone core plugs yielded helium porosity of 10–17% and air permeability of 1–20 mD [*Slater et al*., 2012], but most of them came from intervals characterized by zero or very low transmissivity levels that could not be resolved by in situ hydraulic testing (Figure 10g). These results highlight the importance of the scale of investigation when determining hydraulic properties in these fractured formations. The core samples (~ 2.5 by 5 cm, or 1 by 2 in) targeted coarse-grained intervals devoid of fractures and visible heterogeneities in the core, and therefore, represent small-scale matrix porosity of select sandstone layers. The borehole hydraulic test characterizes formation properties more uniformly with depth and at a scale of meters to tens of meters, representing a combined effect of matrix properties, fractures, and various formation heterogeneities. Since in situ measurements indicate much lower formation permeability than laboratory matrix properties, formation heterogeneities appear to decrease the net effective hydraulic conductivity in these formations. Thus, evaluating formation permeability at the field scale will be particularly important for estimating CO_2 storage potential of this fractured and inhomogeneous formation.

In the South Georgia Rift (SGR), another rift basin on the eastern North American margin evaluated for its CO_2 storage potential, laboratory analysis of porosity and permeably on about a dozen core plugs and sidewall cores is available [*Akintunde et al*., 2014, 2013]. The data suggest that coarse fluvial sandstones have medium to low matrix porosity (2–15%) and low permeability (10^{-3}–10^{-1} mD), attributed to poor sorting, high angularity and small pore throats [*Akintunde et al*., 2013]. In contrast, high porosity (25–35%) and permeability (10–100 mD) were recorded in about half a dozen samples from fine-grained red lacustrine strata, resembling those of the Newark basin [*Akintunde et al*., 2013]. These results suggest finer-grained lacustrine strata may have superior reservoir properties to the coarse-grained fluvial sandstones due to better sorting, and that in the Newark basin, reservoir properties of the finer-grained lacustrine formations should also be evaluated. Furthermore, a separate study focused on tectonic regimes in the SGR basin suggested that those high porosity-permeability lacustrine samples came from a structural block with distinctly different tectonic history, potentially separated from the rest of the basin by a system of faults [*Akintunde et al*., 2014]. Intrabasin faults are also common in the Newark Basin, especially in the central and southern parts [e.g., *Schlische*, 1992]. Therefore, investigating reservoir properties of different structural blocks within the basin may also be important for further work.

Another potential area of interest for further study is the permeability structure within the contact zone of the Palisade Sill and/or near other intrusions within the rift basins. Observations of fractures in the basal contact of the Palisade Sill in the Newark Basin suggest enhanced fracturing near the sill boundary, and potentially, superior hydraulic conductivities of select fractures than in the unaffected sedimentary strata below (Figures 9 and 10). In many parts of the basin, the Palisade Sill occurs at greater depths than described in this study [e.g., *Schlische*, 1992], reaching a depth range that is potentially suitable for supercritical CO_2 storage. Other rift basins on the eastern North American margin, including SGR, host many intrusions belonging to CAMP [e.g., *Schlische et al*., 2003; *Marzoli et al*., 1999], but their hydraulic properties are not yet well characterized. More studies of hydraulic properties of the intrusion boundaries at different depths and in other structural settings will be needed to confirm the hypothesis of higher formation permeability along the intrusion paths. At the same time, our data unambiguously show that the Palisade Sill itself does not contain any hydraulically conductive zones and may thus serve as a caprock for underlying reservoirs (Figure 9). Petrological and petrophysical analysis of diabase sill samples from the SGR basin also showed uniformly low or zero porosity and permeability, suggesting excellent sealing properties [*Akintunde et al*., 2013]. The combination of impermeable diabase overlying transmissive fractures in the basal contact zone of a rift basin intrusion, if sufficient reservoir quality is established in that zone, may provide a suitable reservoir-caprock structure for secure for CO_2 storage.

5. Conclusions

A new set of core and downhole data spanning the Palisade Sill, the marginal Stockton Formation, and the basement unconformity in the northeastern part of the Newark Basin revealed multiple features not observed in outcrops and constrained the lateral variability of basin formations by comparing observations in two close-by wells. Penetration and core recovery in the basement below the Newark Basin showed that crystalline basement consists of grey gneiss, identified as the Fordham Gneiss, similar to that seen in outcrops to the east of the study site, in the Bronx and Westchester County, NY. Crystalline basement is overlain by a thin layer of gravely sandstone followed by a dark purple mudstone unknown age, which is unlike any unit described in the Newark basin to date and potentially corresponds to prerift or early rifting phase deposits. Farther up section, a narrow zone with high uranium concentration identified by anomalously high gamma-ray activity occurs in a setting different from all other known occurrences of uranium in the basin. Unlike those instances, this anomaly is not related to black or dark gray organic-rich layers, but corresponds to dark-red oxidized sandstone. A number of indirect indicators suggest a former redox boundary in this depth, but further geochemical investigation is necessary to identify the origin and magnitude of this uranium anomaly.

The lithological expression of the Stockton Formation at this northeastern edge of the Newark basin differs from the type localities in the central basin. The beds observed in the core are much thinner and are dominated by coarse arkosic sandstones and massive purple and red mudstones. They are representative of the transitional facies between the Stockton and overlying Lockatong Formation, similar to that observed in the

outcrops along the Hudson River in Rockland County, NY and northern Bergen County, NJ. The traditional lithostratigraphic definitions developed in the central basin [*Kümmel*, 1897; *Olsen et al*., 1996] may not be directly applicable at the marginal onlap edges due to differences in depositional environment and structural setting. In addition to a different lithological expression, the marginal facies also exhibit greater lateral heterogeneity. Individual formation members were correlated over large distances (km to 10s of km) in the central Newark basin [*Olsen et al*., 1996; *Kent et al*., 1995]. In this study, individual layers cannot be correlated over the distance of 200 meters (~700 ft) in the bedding dip direction, although the overall lithological expression and bedding parameters are very similar. This direct observation of high lateral variability of the formation strata highlights the challenges of correlating local outcrops without core data.

The new hydraulic data from the two wells constrain aquifer properties in the northern Newark basin at greater depths (>600 ft) than previous groundwater studies [e.g., *Heisig*, 2011]. The same types of water-bearing features were observed as in shallow aquifers of the central and northern Newark basin, dominated by bed-parallel and subvertical transmissive fractures. However, their abundance, continuity, and trasmissivity are significantly decreased at greater depths. Only 4 to 8 narrow hydraulically conductive zones were identified in each of the two wells under injection conditions, none of which measured detectable ambient flow. Some of these zones correspond to steeply dipping fractures close to the Palisade Sill contact, but others appear to be related to bed-parallel fractures or primary matrix porosity. Borehole tests indicate that the majority of intersected strata, including coarse sandstones, do not conduct fluids, although laboratory measurements on some core plugs indicated moderately high porosity and permeability values. Formation heterogeneities, including mineralized and closed fractures, likely decrease the net hydraulic conductivity of these formations, and estimating permeability with borehole hydraulic tests will be essential for determining effective hydrological properties at reservoir depths.

High lateral variability, formation heterogeneity, and limited hydraulic conductivity of the marginal Stockton facies in the Newark Rift Basin may present future challenges for evaluating reservoir and sealing properties of these rocks for geologic storage of CO_2. Similarly, available porosity and permeability data in the South Georgia Basin, another rift basin on the eastern North American margin evaluated for its CO_2 storage potential, suggest that coarse fluvial sandstones have low matrix porosity and may not be ideal for underground injection and storage [*Akintunde et al*., 2013]. Enhanced hydraulic conductivity may potentially exist, however, along buried intrusion boundaries with underlying metasedimentary strata due to thermally enhanced fracturing, e.g., the Palisade Sill contact zone. Overlain by impermeable diabase sills, such zones could potentially provide a suitable reservoir-caprock structure for CO_2 injections if their enhanced permeability is confirmed at other locations, in the Newark basin or near other CAMP intrusions in other rift basins along the eastern North American margin.

Acknowledgments

We gratefully acknowledge TriCarb Consortium for Carbon Sequestration and EPA STAR grant 834503 that supported drilling and logging operations on the Lamont campus. We thank Brian Slater for supervising TW4 core collection, and Chris Lepre for help with core handling and sampling throughout the project. Paul Olsen visually analyzed and described the recovered core. Sally Morgan collected the continuous Multi-Sensor Core Logger (MSCL) scan data at Lamont-Doherty Earth Observatory. Natalia Zakharova and Dennis Kent collected the Spectral Gamma Ray scan data at the Rutgers University, where the TW4 core is now stored in the Newark Basin core archive at the Core Repository. Many thanks go to the members of the EPA STAR project team and Borehole Research Group for assistance during TW3 drilling and hydraulic testing. Special thanks go to Taro Takahashi and Gregory O'Mullan for contributing to planning, execution, and discussion of the EPA STAR project results. We also thank Taro for generously providing thoughtful comments on the manuscript. We gratefully acknowledge Alton Anderson and John Williams from USGS logging services for assistance with hydraulic data acquisition, and for providing interval transmissivity estimates. We also thank Pierre Lacombe and the second anonymous reviewer for providing detailed comments and constructive feedback on the original manuscript. The logging data and field core photo images described in this paper are available in the logging database of the Borehole Research Group at Lamont-Doherty Earth Observatory at http://brg.ldeo.columbia.edu/research_projects/lamont/(last access on 4/12/2016). LDEO Contribution #8014.

References

Abdel-Monem, A. A., and J. L. Kulp (1968), Paleogeography and the source of sediments of the Triassic basin, New Jersey, by K-Ar dating, *Geol. Soc. Am. Bull.*, *79*(9), 1231–1242.

Akintunde, O. M., C. Knapp, and J. Knapp (2013), Petrophysical characterization of the South Georgia Rift Basin for supercritical CO_2 storage: A preliminary assessment, *Environ. Earth Sci.*, *70*(7), 2971–2985.

Akintunde, O. M., C. C. Knapp, and J. H. Knapp (2014), Tectonic significance of porosity and permeability regimes in the red beds formations of the South Georgia Rift Basin, *Tectonophysics*, *632*, 1–7.

Barton, C. A., and M. D. Zoback (1992), Self-similar distribution and properties of macroscopic fractures at depth in crystalline rock in the Cajon Pass Scientific Drill Hole, *J. Geophys. Res.*, *97*, 5181–5200, doi:10.1029/91JB01674.

Barton, M. D., J.-M. Staude, E. A. Snow, and D. A. Johnson (1991), Aureole systematics, *Rev. Mineral.*, *26*(1), 723–847.

Blackburn, T. J., P. E. Olsen, S. A. Bowring, N. M. McLean, D. V. Kent, J. Puffer, G. McHone, E. T. Rasbury, and M. Et-Touhami (2013), Zircon U-Pb geochronology links the end-Triassic extinction with the Central Atlantic Magmatic Province, *Science*, *340*(6135), 941–945.

Blum, P., A. Rabaute, P. Gaudon, and J. F. Allan (1997), Analysis of natural gamma-ray spectra obtained from sediment cores with the shipboard scintillation detector of the Ocean Drilling Program: Example from leg 156, *Proc. Ocean Drill. Program Sci. Results*, *156*, 183–195.

Cornet, B., and P. E. Olsen (1985), A summary of the biostratigraphy of the Newark Supergroup of eastern North America, with comments on early Mesozoic provinciality, in *Simposio Sobre Floras del Triassico Tardio, su Fitogeografia y Palecologia: Memoria, III Congresso Latinoamericano de Paleontologia, Mexico*, edited by R. Weber, pp. 67–81, Univ. Natl. Autonomf de Mexico, Inst. de Geol., Mexico City.

Costain, J. K., and C. Coruh (1989), Tectonic setting of Triassic half-grabens in the Appalachians: Seismic data, acquisition, processing and results, in *Extentional Tectonics and Stratigraphy of the North Atlantic Margins, AAPG Mem. 46*, edited by A. J. Tankard and H. R. Balkwill, pp.155–174, Amer. Assoc. Petrol. Geol., Tulsa, Okla.

Day-Lewis, F. D., C. D. Johnson, F. L. Paillet, and K. J. Halford (2011), *FLASH: A Computer Program for Flow-Log Analysis of Single Holes*., U.S. Geol. Surv., Storrs Mansfield, CT. [Available at http://water.usgs.gov/ogw/flash/, last accessed 12 Sept. 2015.]

Drake, A. A., R. A. Volkert, D. H. Monteverde, G. C. Herman, H. F. Houghton, R. A. Parker, and R. F. Dalton (1996), *Bedrock Geologic Map of Northern New Jersey*, U.S. Dep. of the Inter., U.S. Geol. Surv., Reston, Va.

El-Tabakh, M., R. Riccioni, and B. C. Schreiber (1997), Evolution of late Triassic rift basin evaporites (Passaic Formation): Newark Basin, Eastern North America, *Sedimentology*, *44*(4), 767–790.

Goldberg, D. S., and K. Burgdorff (2005), Natural fracturing and petrophysical properties of the Palisades dolerite sill, in *Petrophysical Properties of Crystalline Rocks*, edited by P. K. Harvey et al., pp. 25–36, Geol. Soc., London, doi:10.1144/gsl.sp.2005.240.01.03.

Goldberg, D. S., T. Lupo, M. Caputi, C. A. Barton, and L. Seeber (2003), Stress regimes in the Newark basin rift: Evidence from core and downhole data, in *The Great Rift Valleys of Pangea in Eastern North America*, edited by P. M. LeTourneau and P. E. Olsen, pp. 104–117, Columbia Univ. Press, N. Y.

Goldberg, D. S., D. V. Kent, and P. E. Olsen (2010), Potential on-shore and off-shore reservoirs for CO_2 sequestration in Central Atlantic magmatic province basalts, *Proc. Natl. Acad. Sci. U. S. A.*, *107*(4), 1327–1332.

Hanson, R. B. (1995), The hydrodynamics of contact metamorphism, *Geol. Soc. Am. Bull.*, *107*(5), 595–611, doi:10.1130/0016-7606(1995)107<0595:thocm>2.3.co;2.

Hanson, R. B., and M. D. Barton (1989), Thermal development of low-pressure metamorphic belts: Results from two-dimensional numerical models, *J. Geophys. Res.*, *94*, 10,363–10,377, doi:10.1029/JB094iB08p10363.

Heisig, P. M. (2011), *Water Resources of Rockland County, New York, 2005-07, With Emphasis on the Newark Basin Bedrock Aquifer*, U. S. Geol. Surv., Reston, Va. [Available at http://ny.water.usgs.gov/projects/rockland/, last accessed 23 Feb. 2016.]

Herman, G. C. (2010), Hydrogeology and Borehole geophysics of fractured-bedrock aquifers, Newark Basin, New Jersey, in *Contributions to the Geology and Hydrogeology of the Newark Basin, (2010)*, edited by G. C. Herman, State of N. J., Dep. of Environ. Prot., Water Resour. Manage., N. J. Geol. Surv., Ewing Township, N. J .

Herman, G. C. (2009), Steeply-dipping extension fractures in the Newark basin, New Jersey, *J. Struct. Geol.*, *31*(9), 996–1011, doi:10.1016/j.jsg.2008.10.008.

Hostetler, P. B., and R. M. Garrels (1962), Transportation and precipitation of uranium and vanadium at low temperatures, with special reference to sandstone-type uranium deposits, *Econ. Geol.*, *57*(2), 137–167.

Houghton, H. (1990), Hydrogeology of the early mesozoic rocks of the Newark Basin, New Jersey, in *Proceedings: Aspects of Ground-water in New Jersey*, edited by R. L. Kroll, and J. O. Brown, Geological Assc. of New Jersey 7th Annual Meeting, pp. E1–E36, Kean College of New Jersey, Union, N. J.

Hubbert, M. K., and D. G. Willis (1957), Mechanics of hydraulic fracturing, *Trans. Am. Inst. Min. Metall. Pet. Eng.*, *210*, 153–168.

Intergovernmental Panel on Climate Change (IPCC) (2005), Carbon dioxide capture and storage, special report, Prepared by Working Group III of the Intergovernmental Panel on Climate Change, Cambridge University Press, Cambridge, U. K.

Isler, D. E., Vellone, D. A., Merguerian, Charles, and Merguerian, J. M. (2009), Redefining the southern terminus of the intrusive contact between the Yonkers and Fordham gneiss in Van Cortlandt Park, New York City, NY: in *Sixteenth Annual Conference on Geology of Long Island and Metropolitan New York*, *Long Island Geol. Program with Abstracts*, edited by G. N. Hanson, 15 p., State Univ. of N. Y., Stony Brook.

Jensen, M. L. (1958), Sulfur isotopes and the origin of sandstone-type uranium deposits [Colorado Plateau and Wyoming], *Econ. Geol.*, *53*(5), 598–616.

Kent, D. V., P. E. Olsen, and W. K. Witte (1995), Late Triassic-earliest Jurassic geomagnetic polarity sequence and paleolatitudes from drill cores in the Newark rift basin, eastern North America, *J. Geophys. Res.*, *100*, 14,965–914,998.

Kümmel, H. B., (1897), The Newark System or red sandstone belt, in New Jersey Geological Survey *Annual Report of the State Geologist for the Year of 1897*, pp. 23–159.

Kümmel, H. B. (1898), The Newark System or red sandstone belt, in New Jersey Geological Survey *Annual Report of the State Geologist for the Year of 1897*, pp. 23–159.

Kümmel, H. B. (1899), The Newark or red sandstone rocks of Rockland County, New York, in 18th New Jersey Geological Survey *Annual Report of the State Geologist for the Year of 1897*, pp. 9–50.

Lackner, K. S. (2003), Climate change: A guide to CO_2 sequestration, *Science*, *300*(5626), 1677–1678, doi:10.1126/science.1079033

Lacombe, P. J., and W. C. Burton (2010), Hydrogeologic framework of fractured sedimentary rock, Newark Basin, New Jersey, *Ground Water Monit. Rem*, *30*(2), 35–45.

Lanci, L., D. V. Kent, and K. G. Miller (2002), Detection of Late Cretaceous and Cenozoic sequence boundaries on the Atlantic coastal plain using core log integration of magnetic susceptibility and natural gamma ray measurements at Ancora, New Jersey, *J. Geophys. Res.*, *107*(B10), 2216, doi:10.1029/2000JB000026.

Litynski, J., et al. (2009), US Department of Energy's regional carbon sequestration partnership program: Overview, *Energy Procedia*, *1*(1), 3959–3967.

Malinconico, M. L. (2009), Synrift to early postrift basin-scale groundwater history of the Newark basin based on surface and borehole vitrinite reflectance data, in *Contributions to the Geology and Hydrogeology of the Newark Basin*, edited by G. C. Herman, N. J. Geol. Surv., Ewing Township, *Geol. Surv. Bull.*, *77*, pp. C1–C38, N. J.

Marzoli, A., P. R. Renne, E. M. Piccirillo, M. Ernesto, G. Bellieni, and A. De Min (1999), Extensive 200-million-year-old continental flood basalts of the Central Atlantic Magmatic Province, *Science*, *284*(5414), 616–618.

Matter, J. M., D. Goldberg, R. Morin, and M. Stute (2006), Contact zone permeability at intrusion boundaries: New results from hydraulic testing and geophysical logging in the Newark Rift Basin, New York, USA, *Hydrogeol. J.*, *14*(5), 689–699, doi:10.1007/s10040-005-0456-3.

Matter, J. M., T. Takahashi, and D. S. Goldberg (2007), Experimental evaluation of in situ CO_2-water-rock reactions during CO_2 injection in basaltic rocks: Implications for geological CO_2 sequestration, *Geochem. Geophys. Geosyst.*, *8*, Q02001, doi:10.1029/2006GC001427.

Merguerian, Ch., and J. E. Sanders (1995), Late syn-intrusive clastic dikes at the base of the Palisades intrusive sheet, Fort Lee, NJ, imply a shallow (~3 to 4 km) depth of intrusion, in *Geology of Long Island and metropolitan New York, Long Island Geol. Program with Abstr.*, edited by G. N. Hanson,135 p., State Univ. of N. Y., Stony Brook.

Michalski, A., and R. Britton (1997), The role of bedding fractures in the hydrogeology of sedimentary bedrock—Evidence from the Newark Basin, New Jersey, *Ground Water*, *35*(2), 318–327, doi:10.1111/j.1745-6584.1997.tb00089.x.

Morin, R. H., G. B. Carleton, and S. Poirier (1997), Fractured-aquifer hydrogeology from geophysical logs: The Passaic Formation, New Jersey, *Ground Water*, *35*(2), 328–338, doi:10.1111/j.1745-6584.1997.tb00090.x.

Morin, R. H., L. A. Senior, and E. R. Decker (2000), Fractured-aquifer hydrogeology from geophysical logs: Brunswick Group and Lockatong Formation, Pennsylvania. *Ground Water*, *38*(2), 182–192.

Olsen, P. E. (1980), The Latest Triassic and Early Jurassic Formations of the Newark Basin, Eastern North America, Newark Supergroup: Stratigraphy, Structure, and Correlation, N. J. Acad. of Sci., Bulletin, vol. 25, pp. 25–51.

Olsen, P. E. (1986), A 40-million-year lake record of early Mesozoic orbital climatic forcing, *Science*, *234*(4778), 842–848.

Olsen, P. E., and D. V. Kent (1996), Milankovitch climate forcing in the tropics of Pangaea during the Late Triassic, *Palaeogeogr. Palaeoclimatol. Palaeoecol.*, *122*(1), 1–26.

Olsen, P. E., and E. C. Rainforth (2001), The "Age of Dinosaurs" in the Newark basin, with special reference to the lower Hudson Valley, in *Geology of the Lower Hudson Valley, 2001 New York State Geological Association Field Trip Guide Book, vol. 73*, edited by A. E. Gates, pp. 59–176, N. Y. State Geol. Assoc., N. Y. State Museum, Albany.

Olsen, P. E., R. W. Schlische, and P. Gore (Eds.) (1989), Tectonic, depositional, and pleoecological history of early Mesozoic Rift Basins, Eastern North America, AGU Guidebk., T351, 1–174.

Olsen, P. E., D. V. Kent, B. Cornet, W. K. Witte, and R. W. Schlische (1996), High-resolution stratigraphy of the Newark rift basin (early Mesozoic, eastern North America), *Geol. Soc. Am. Bull.*, *108*(1), 40–77.

Olsen, P. E., M. O. Withjack, R. W. Schlishe, D. S. Goldberg, D. V. Kent, K. Tamulonis, M. Coueslan, and D. J. Collins (2011b), Subsurface images of the northern Newark Basin, New York, USA and their implications for carbon sequestration, Abstract GC44A-07 presented at 2011 Fall Meeting, AGU, San Francisco, Calif., 5–9 Dec.

O'Mullan, G., M. E. Dueker, K. Clauson, Q. Yang, K. Umemoto, N. Zakharova, J. Matter, M. Stute, T. Takahashi, and D. Goldberg (2015), Microbial stimulation and succession following a test well injection simulating CO_2 leakage into a shallow newark basin aquifer, *PloS One*, *10*(1), e0117812.

Puffer, J. H., K. A. Block, and J. C. Steiner (2009), Transmission of flood basalts through a shallow crustal sill and the correlation of sill layers with extrusive flows: The Palisades intrusive system and the basalts of the Newark Basin, New Jersey, USA, *J. Geol.*, *117*(2), 139–155.

Reynolds, D. J. (1994), Sedimentary basin evolution: Tectonic and climatic interaction, PhD thesis, Columbia Univ., N. Y.

Rodosta, T., et al. (2011), US Department of Energy's regional carbon sequestration partnership initiative: Update on validation and development phases, *Energy Procedia*, *4*, 3457–3464.

Savage, E. L. (1968), The Triassic rocks of the northern Newark Basin, in *Guidebook to field excursions* (RM Finks, ed.), NY State Geol. Ass., 40th Annu. Meet., Flushing, N. Y.

Schlische, R. W. (1992), Structural and stratigraphic development of the Newark extensional basin, eastern North America: Evidence for the growth of the basin and its bounding structures, *Geol. Soc. Am. Bull.*, *104*(10), 1246–1263, doi:10.1130/0016-7606(1992)104<1246:sasdot>2.3.co;2.

Schlische, R. W., M. O. Withjack, and P. E. Olsen (2003), Relative timing of CAMP, rifting, continental breakup, and basin inversion: Tectonic significance, in *The central Atlantic Magmatic Province: Insights From Fragments of Pangea, Geophys. Monogr.*, pp. 33–59, AGU, Washington, D. C.

Shao, A. (2011), Chemistry of the Newark Basin in Context of Vulnerability to CO_2 Leak, *Senior Thesis, Environ. Biology*, Barnard College, N.Y.

Slater, B. E., L. Smith, M. P. Tymchak, and D. J. Collins (2012), Preliminary results from the TriCarb deep stratigraphic well drilled into the Newark Rift Basin, Rockland County, NY, paper presented at the 41st Annual Eastern Section AAPG Meeting, AAPG, Cleveland, Ohio, 22–26 Sept.

Smoot, J. P. (1991), Sedimentary facies and depositional environments of early Mesozoic Newark Supergroup basins, eastern North America, *Palaeogeogr. Palaeoclimatol. Palaeoecol.*, *84*, 369–423.

Smoot, J. P. (2010), Chapter A: Triassic depositional Facies in the Newark Basin. Contributions to the geology and hydrogeology of the Newark basin, *N. J. Geol. Surv. Bull.*, *77*, A1–A110.

Spirakis, Ch. S. (1996), The roles of organic matter in the formation of uranium deposits in sedimentary rocks, *Ore Geol. Rev.*, *11.1*, 53–69.

Terzaghi, R. D. (1965), Sources of error in joint surveys, *Géotechnique*, *15*(3), 287, doi:10.1680/geot.1965.15.3.287.

Turner-Peterson, Ch. E. (1980), Sedimentology and uranium mineralization in the Triassic-Jurassic Newark basin, Pennsylvania and New Jersey, in *Uranium in Sedimentary Rocks: Applications of the Facies Concept to Exploration*, edited by C. M. Turner-Peterson, pp. 149–76, SEPM, Rocky Mt. Sect., Short Course Notes, Denver, Colo.

Tymchak, M. P., D. J. Collins, C. B. Brown, J. Conrad, P. W. Papadeas, M. L. Coueslan, K. Tamulonis, D. S. Goldberg, and P. E. Olsen (2011), New seismic reflection profiling across the northern Newark Basin USA: Data acquisition and preliminary results, Abstract GC51B-0979 presented at 2011 Fall Meeting, AGU, San Francisco, Calif., 5–9 Dec.

Van Houten, F. B. (1969), Late Triassic Newark Group, northcentral New Jersey and adjacent Pennsylvania and New York, in *Geology of Selected Areas in New Jersey and Eastern Pennsylvania and Guidebook of Excursions, New Brunswick, New Jersey, Geological Society of America, Field Trip, 4*, edited by S. Subitzki, pp. 314–347, Rutgers Univ. Press, Atlantic City, N. J.

Withjack, M. O., R. W. Schlische, M. L. Malinconico, and P. E. Olsen (2013), Rift-basin development: Lessons from the Triassic–Jurassic Newark Basin of eastern North America, *Geol. Soc. Spec. Publ.*, *369*(1), 301–321.

Yager, R. M., and N. M. Ratcliffe (2010), Hydrogeology and simulation of groundwater flow in fracturedrock in the Newark basin, Rockland County, New York, U.S. Geol. Surv. Sci. Invest. Rep., 2010–5250, 139 p.

Yang, Q., et al. (2014), Groundwater hydrogeochemistry in injection experiments simulating CO_2 leakage from geological storage reservoir, *Int. J. Greenhouse Gas Control*, *26*, 193–203.

Yilmaz, H. (1981), Genesis of uranium deposits in Neogene sedimentary rocks overlying the Menderes metamorphic massif, Turkey, *Chem. Geol.*, *31*, 185–210.